AD-A156 932 IN SITU STUDIES OF ENERGY DEPOSITION BY ION BEAMS(U) 1/1
CONNECTICUT UNIV STORRS DEPT OF PHYSICS
J I BUDNICK ET AL. 14 JUN 85 N00014-80-C-0910
UNCLASSIFIED F/G 20/12 NL

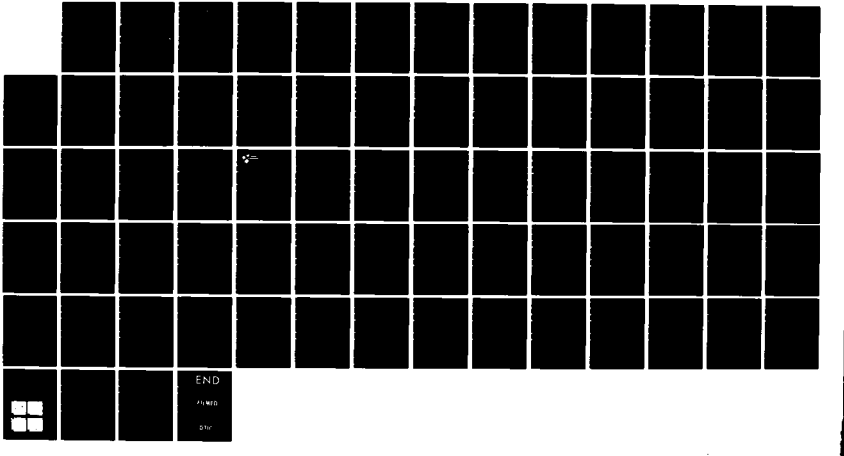

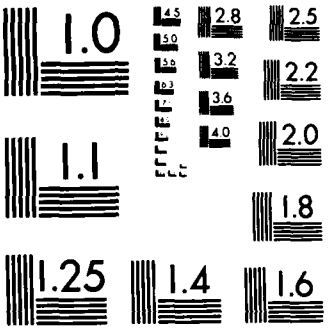

MICROCOPY RESOLUTION TEST CHART

Office of Naval Research

Final Technical Report

September 1, 1980 - August 31, 1983

"In Situ Studies of Energy Deposition by Ion Beams"

ONR Contract No. N00014-80-C-0910

Major Investigators:

J. I. Budnick, F. P. Lipschultz and F. Namavar
University of Connecticut
Storrs, CT 06268

F. A. Otter and T. W. Grudkowski
United Technologies Research Center
East Hartford, CT 06108

June 14, 1985

SECURITY CLASSIFICATION OF THIS PAGE (When Data Entered)

REPORT DOCUMENTATION PAGE	READ INSTRUCTIONS BEFORE COMPLETING FORM
1. REPORT NUMBER	2. GOVT ACCESSION NO. AD-A156932 — 3. RECIPIENT'S CATALOG NUMBER
4. TITLE (and Subtitle) In Situ Studies of Energy Deposition by Ion Beams.	5. TYPE OF REPORT & PERIOD COVERED Final Technical Report: 9/1/80 - 8/31/83 6. PERFORMING ORG. REPORT NUMBER
7. AUTHOR(s) J. I. Budnick, F. P. Lipschultz, F. Namavar, F. A. Otter and T. W. Grudkowski	8. CONTRACT OR GRANT NUMBER(s) ONR No. N00014-80-C-0910
9. PERFORMING ORGANIZATION NAME AND ADDRESS Department of Physics University of Connecticut Storrs, CT 06268	10. PROGRAM ELEMENT, PROJECT, TASK AREA & WORK UNIT NUMBERS
11. CONTROLLING OFFICE NAME AND ADDRESS Office of Naval Research Physics Division Office (Code 412) 800 North Quincy Street Arlington, Virginia 22217	12. REPORT DATE June 14, 1985 13. NUMBER OF PAGES 31 & publ. attached
14. MONITORING AGENCY NAME & ADDRESS(if different from Controlling Office)	15. SECURITY CLASS. (of this report) 15a. DECLASSIFICATION/DOWNGRADING SCHEDULE
16. DISTRIBUTION STATEMENT (of this Report)	
17. DISTRIBUTION STATEMENT (of the abstract entered in Block 20, if different from Report)	
18. SUPPLEMENTARY NOTES	
19. KEY WORDS (Continue on reverse side if necessary and identify by block number) ion implantation Ion beam mixing Rutherford Backscattering surface acoustic waves ion beam damage laser irradiation of surface acoustic wave system nuclear resonance profiling	
20. ABSTRACT (Continue on reverse side if necessary and identify by block number) This report summarizes the results of initial surface acoustic wave studies on a variety of systems including lithium niobate ($LiNbO_3$), quartz (SiO_2), silicon on $LiNbO_3$, silicon on SiO_2 and silicon on sapphire, which have been subjected to ion implantation and to visible laser irradiation. In addition, results of ion beam mixing studies on the Al-Si system are reported, as well as the application of nuclear resonance profiling to a study of the near surface aluminum distribution in silicon.	

DD FORM 1 JAN 73 1473 EDITION OF 1 NOV 65 IS OBSOLETE
S/N 0102-014-6601

SECURITY CLASSIFICATION OF THIS PAGE (When Data Entered)

Table of Contents

A. Surface Acoustic Wave Studies

I. INTRODUCTION:

Studies of the effects of energy deposition on piezoelectric substrates (both uncoated and coated with silicon thin films) have been performed using several different techniques for the analyses of the phenomena occurring during energy deposition and the subsequent material property changes. An outline of the details of these studies now follows:

1) Forms of energy deposited:
   a. Energetic ion beams (40 to 120 keV)
   b. Visible laser light (0 to 3 watts)
2) Substrates (piezoelectric):
   a. Lithium niobate (uncoated)
   b. Quartz (uncoated)
   c. Lithium niobate (coated with a polycrystalline silicon thin film)
   d. Quartz (coated with a polycrystalline silicon thin film)
   e. Silicon on sapphire (not piezoelectric)
3) Analytic techniques:
   a. The attenuation of surface acoustic waves (S.A.W.s - 200 MHz) measured in situ during energy deposition
   b. The attenuation of S.A.W.s as a function of temperature
   c. The analysis of implant damage using:

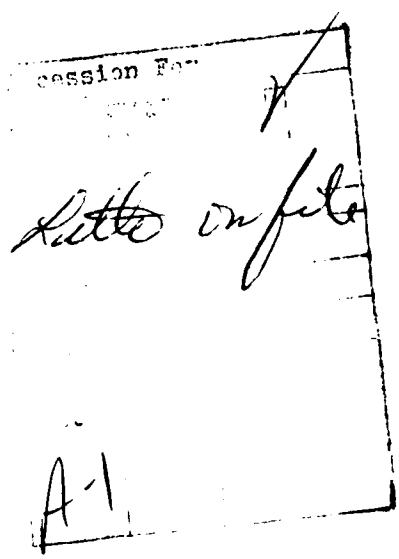

i. Rutherford Back Scattering

ii. Electron beam microprobe analysis

iii. X-ray diffraction studies.

To one degree or another, all of these measurements represent initial studies of these systems. In some cases, tentative remarks about the phenomena being observed may be advanced, but additional work must be carried out to remove the speculative nature of these remarks. In any event more work remains to be done; further studies are being carried out.

II. EXPERIMENTAL OBSERVATION:

1. In Situ Ion Implantation Studies Using Surface Acoustic Wave Attenuation.

The effects of energetic ion beams (ion kinetic energies in the range of 40 to 120 keV; most studies at 100 keV) on the surface properties of piezoelectric substrates have been conducted using the attenuation of surface acoustic waves as a probe of the changes to the surface of the sample. Nearly all of the energy associated with the S.A.W. is confined to within one acoustic wavelength of the surface (typically, a distance of 10 micrometers), and hence these waves are well-suited to study ion implantation-induced surface changes. The substrates have been the piezoelectric materials, quartz and lithium niobate.[1] (While these materials are interesting technical substances in their own right, their piezoelectric properties were important to the fabrication of S.A.W. transducers.) In our studies the implanted regions of these materials were both uncoated and coated with a thin film of polycrystalline silicon. Preliminary studies have been carried out with a number of different ion species (argon, boron, chlorine, phosphorous, oxygen); the

majority of cases were done with argon ions because of the chemical inertness of argon and its moderate penetration depth. Several runs were done using phosphorous ions because of their chemical reactivity. Typical ion current densities were estimated to be about 6*10^(-6) A/cm^2 , although some runs were done with ion current densities on the order of 6*10^(-7) A/cm^2 .

The acoustic attenuation apparatus we use measures the change in attenuation versus time. What is seen for uncoated samples is an increase in attenuation (a decrease in the received acoustic signal) upon beginning the ion implant, followed by a partial recovery of the acoustic signal upon ceasing the ion implant. (See Figure 1.) This is to be contrasted with what is seen for samples with silicon thin films. At the very beginning of the ion implant (e. g. no prior implantation has taken place), a phosphorous beam of about 6*10^(-6) A/cm^2 at 100 keV produces a large (about 20 dB/cm), rapid, permanent increase in the attenuation. (See Figure 2.) The polycrystalline silicon film/piezoelectric substrate combination appears to be quite sensitive to ion implantation. Upon resuming ion implantation, there is an initial, modest increase in the attenuation, followed quickly by a partial recovery in the acoustic signal. Upon ceasing the ion implant, there is a prompt, sizable increase in the acoustic attenuation, with the increased attenuation being permanent. (See Figure 3.)

These phenomena are dependent on the several variables in this experiment: ion kinetic energy, ion current density, implant history, ion species, sample substrate. It has not been possible to vary all of these parameters in a systematic manner to obtain a definitive picture of what is

happening. However in section **III**, several tentative models are proposed based on the above observations and those presented in section 2 below.

2. In Situ Laser Illumination Studies Using Surface Acoustic Wave Attenuation.

Most of the S.A.W. samples also have been exposed to intense monochromatic laser light. The variables in this case are: substrate material (quartz or lithium niobate); the surface is uncoated or coated with silicon; the illuminated region was previously implanted or unimplanted; light intensity; light wavelength; light intensity constant (DC) or chopped at 440 Hz (AC). As before, it has not been possible to adjust all of the variables to a sufficient degree so that a concise picture emerges. However some remarks about phenomena observed may be made and some tentative conclusions drawn (see below and section **III**).

In the case of uncoated samples, the unimplanted regions are clear and absorb very little of the light; a small fraction of the light is reflected at the surface, due to the change in refractive index (air to crystal) and from the aluminum sample holder beneath the sample. As might be expected, little change in the acoustic attenuation is seen upon starting or ceasing illumination of the acoustic path. However, there is some evidence of a rapid, small increase in the attenuation for lithium niobate upon starting the illumination of the sample, which suggests an opto-elastic interaction - perhaps some change in the elastic constants of lithium niobate upon exposure to light. (See Figure 4.)

The implanted regions on the uncoated substrates are darkened by the ion implant and absorb a fraction of the incident light. The following description is typical of what is observed upon exposing the implanted

region to laser light. At the instant the optical beamstop is removed, there is a rapid (time constant of about 3-4 seconds) but moderate (a few dB/cm increase) rise in the attenuation, followed by a very small, slow drift upwards in attenuation (this latter effect appears to be due to a heating of the entire sample). Upon putting the beamstop in front of the light beam there is a similar, rapid (3 to 4 second time constant) recovery of the acoustic signal. The recovery is essentially complete, aside from the offset in attenuation (of a few tenths of a dB/cm) which matches the smaller attenuation increase due to the heating drift. (See Figure 5.)

It is possible that heating of the entire sample affects the attenuation by one or more mechanisms: 1) a dependence of the attenuation coefficient of the implanted region and/or the bulk substrate on the temperature of the sample; 2) a detuning of the resonant structure of the S.A.W. transducers due to thermal expansion of the sample. In any event, it is a fairly small effect here. The more prominent effect (the rapid increase in attenuation of several dB/cm) may be due to a rapid temperature rise due to heating of the darkened implanted thin layer and/or the generation of mobile charge carriers in the implanted region by the light. The temperature rise could change the elastic constants of the implanted region or change the electrical conductivity of the thin surface layer. The generation of charge carriers would also be expected to change the electrical conductivity of the implanted region. A conducting layer on the surface of the piezoelectric substrate might be expected to interact with the electromagnetic component of the traveling acoustic wave and damp that wave due to the generation of Joule heat from the induced currents. Our present inability to measure acoustic attenuation at several acoustic

frequencies simultaneously or to measure the velocity change of the acoustic waves precludes resolving the question of which model is correct.

More detailed analyses of the rise-time of the acoustic attenuation change as a function of light intensity and light wavelength shows that the risetime (and falltime) of the attenuation is essentially independent of light intensity and light wavelength. The height of the attenuation change appears to be a linearly increasing function of the light intensity, although there possibly is a threshold of a small fraction of a watt/cm^2; the height appears to be independent of the light wavelength. (See Figure 6.) The quartz and lithium niobate samples coated with a thin film of polycrystalline silicon are dark gray, hence a fraction of the laser illumination is absorbed. In situ acoustic attenuation measurements of the effects of steady, intense light (of intensity of the order of a few watts per cm^2) show a similar behavior. Intensities of one watt/cm^2 or greater show a positive change in attenuation upon exposure to light. The change in attenuation increases with increasing intensity. However for intensities below one watt/cm^2, there is a negative change in attenuation upon exposure to light. It is possible this latter effect is simply due to a thermal expansion from heating: the device is tuned through a peak in the resonance curve of the transducer and for a small amount of heating the signal improves. However, the effect is moderately big and has a short time constant (a few seconds), which would tend to discount detuning from thermal expansion as the sole source of this attenuation change. Further work remains to be done to determine that this is a significant effect.

If the laser light is chopped (at 440 Hz) rather than held steady, and the acoustic signal that is detected is the AC (440 Hz) modulation that

then appears on an otherwise steady RF carrier, a small but measurable change in the attenuation is seen upon exposure to the chopped light. (See Figure 7.) So far our observations are qualitative, but the existence of this AC effect would seem to suggest an opto-electronic interaction rather than a purely thermal effect. More quantatative measurements need to be carried out.

III. POSSIBLE MODELS:

There are a variety of mechanisms which could change the strength of the received RF signal at the RF amplifier and thus affect the reading of the relative attenuation that we measure. Some of the mechanisms could be due to significant physical phenomena which occur in the acoustic path and are the real effects we are looking for. Some of the mechanisms could be due to changes in the transducer characteristics or shifts in the electronics, hence they should be classified as spurious effects. Both real and spurious effects are occurring to one degree or another, and we shall now attempt to separate the two and discuss possible mechanisms leading to the real effects.

1. Spurious Effects.

Due to the limitations on the available electronics, what is measured is a change in the attenuation of the acoustic signal rather than an absolute insertion loss. As a result, change in the output voltage or frequency of the RF signal generator, change in the gain or tuning of the RF receiver, change in the S.A.W. transducer characteristic, or change in the connecting cables (e.g., a change in the impedance characteristic at an RF connector) all show up as change in the received signal strength through the sample channel and hence as an apparent change in the relative attenuation of the sample being studied. The acoustic properties of the sample region might not have changed, although the received RF signal has changed, hence this attenuation change is described as spurious.

The available electronics are moderately stable. Small shifts in the RF output of the signal generator have been noted, but these should amount to a slow drift of a decibel or two. The RF frequency is usually

monitored, and while there are small shifts in RF frequency, these would lead to a small drift in the relative attenuation of a decibel or two. The receiver characteristics are more difficult to account for, but tuning and gain appear to be reasonably stable. The interconnecting cables usually aren't disturbed during a run, so the remaining variables are the behavior of the S.A.W. transducers and the sample. Change in the received RF signal that appears to be related to change in the transducers has been seen, but it is difficult to account for just what is causing this shift in signal level. Change in the temperature of the sample changes the behavior of the transducers, but not in a predictable manner. One measurement of the attenuation change as a function of temperature showed a negligible attenuation shift (about 1 dB) over the temperature range of -50 Celcius to +50 Celcius. Using a somewhat different technique to measure attenuation change in warming from +18 C to +50 C yielded an increase in attenuation of about 7 dB which remained on cooling to room temperature. Furthermore, retuning the RF oscillator and receiver did not change the received signal much, hence we were left with an unaccounted for shift in the transducer characteristic.

There are several pieces of evidence which suggest that most of the change in attenuation seen during ion implantation and exposure to light is not due to spurious thermal effects. The first observation involves the measured attenuation change as a function of the absorbed power in the [illegible] light beam. The total ion current reaching the sample is typically some microamps accelerated across a potential difference of 100 kV. This corresponds to an incident power of 0.1 watts reaching the sample surface from the ion beam. Attenuation changes have been as great as 10 to

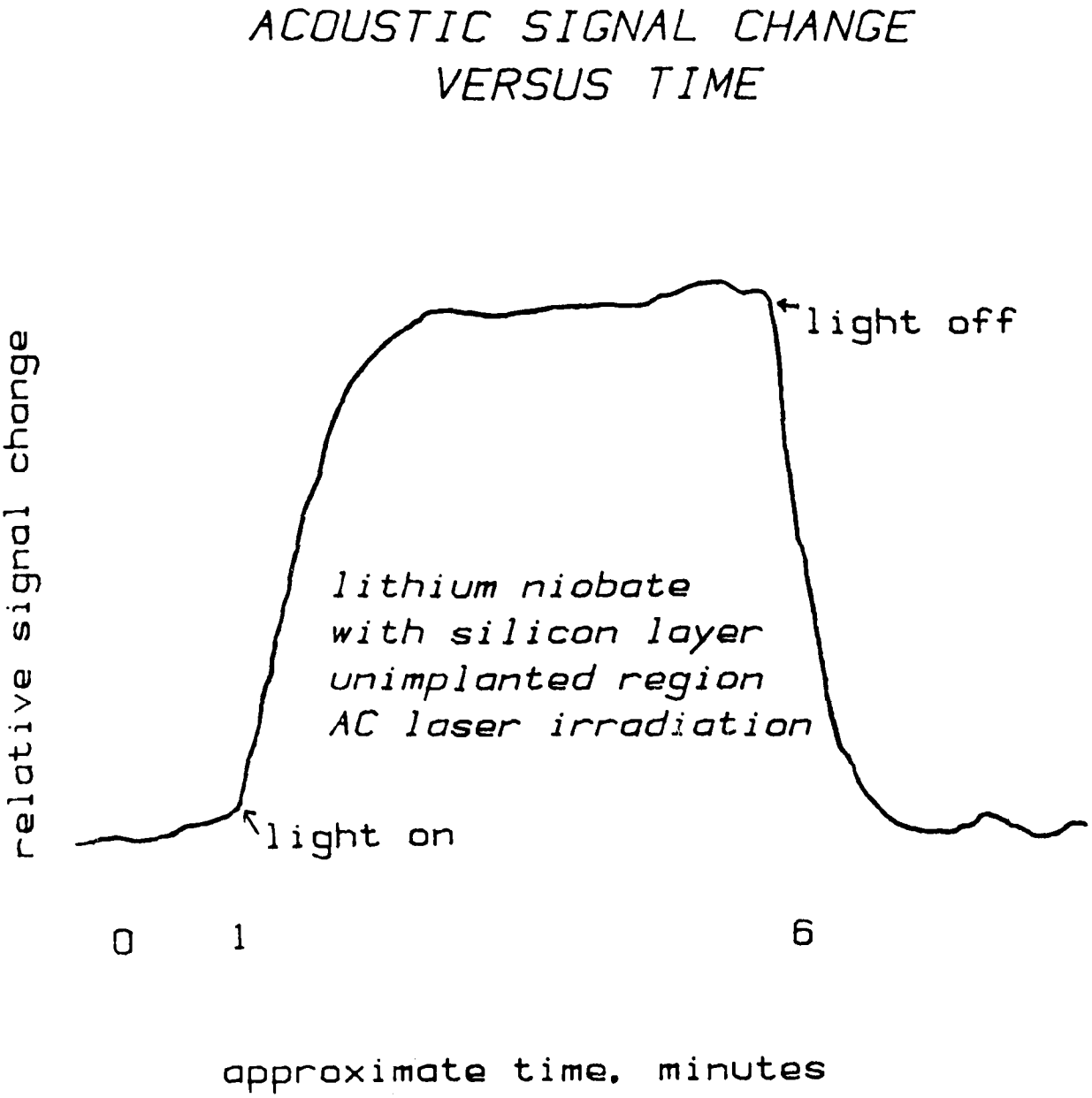
ACOUSTIC SIGNAL CHANGE
VERSUS TIME
relative signal change
light off
lithium niobate
with silicon layer
unimplanted region
AC laser irradiation
light on
0
1
6
approximate time, minutes

Figure 7

ACOUSTIC ATTENUATION CHANGE VERSUS LIGHT POWER

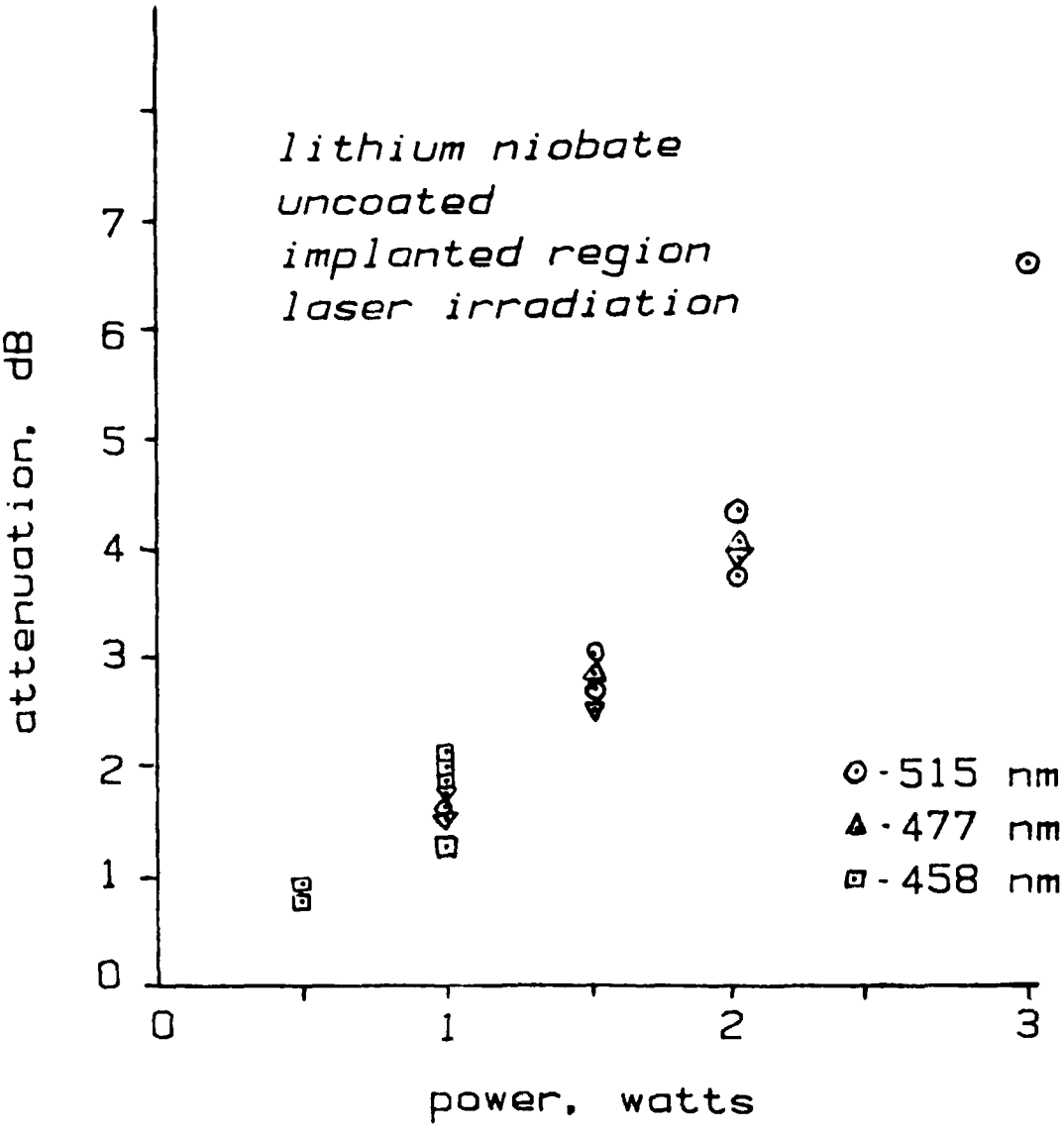

Figure 6

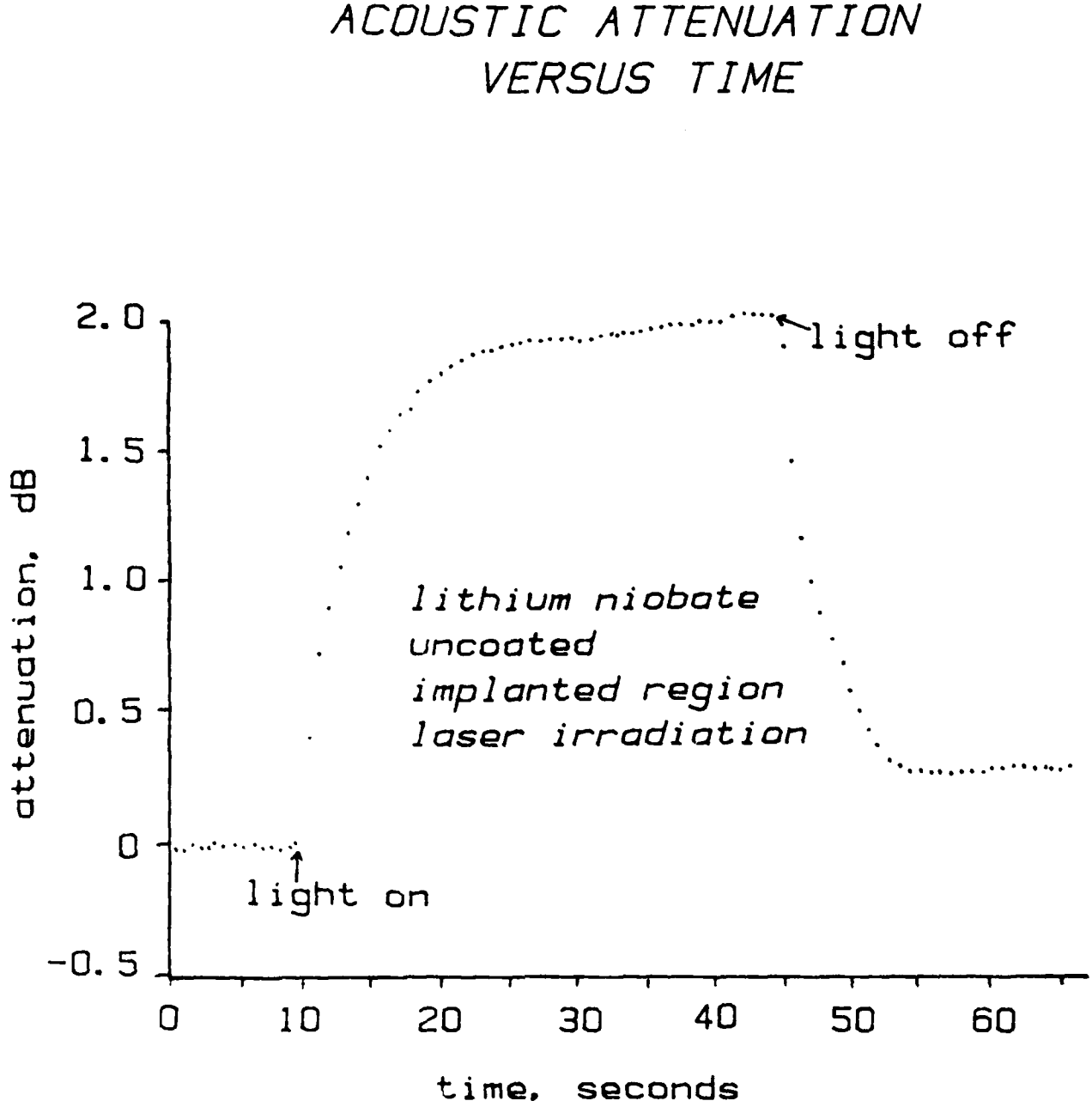
ACOUSTIC ATTENUATION
VERSUS TIME
2.0
1.5
1.0
0.5
0
-0.5
attenuation, dB
light off
lithium niobate
uncoated
implanted region
laser irradiation
light on
0
10
20
30
40
50
60
time, seconds

Figure 5

ACOUSTIC ATTENUATION VERSUS TIME

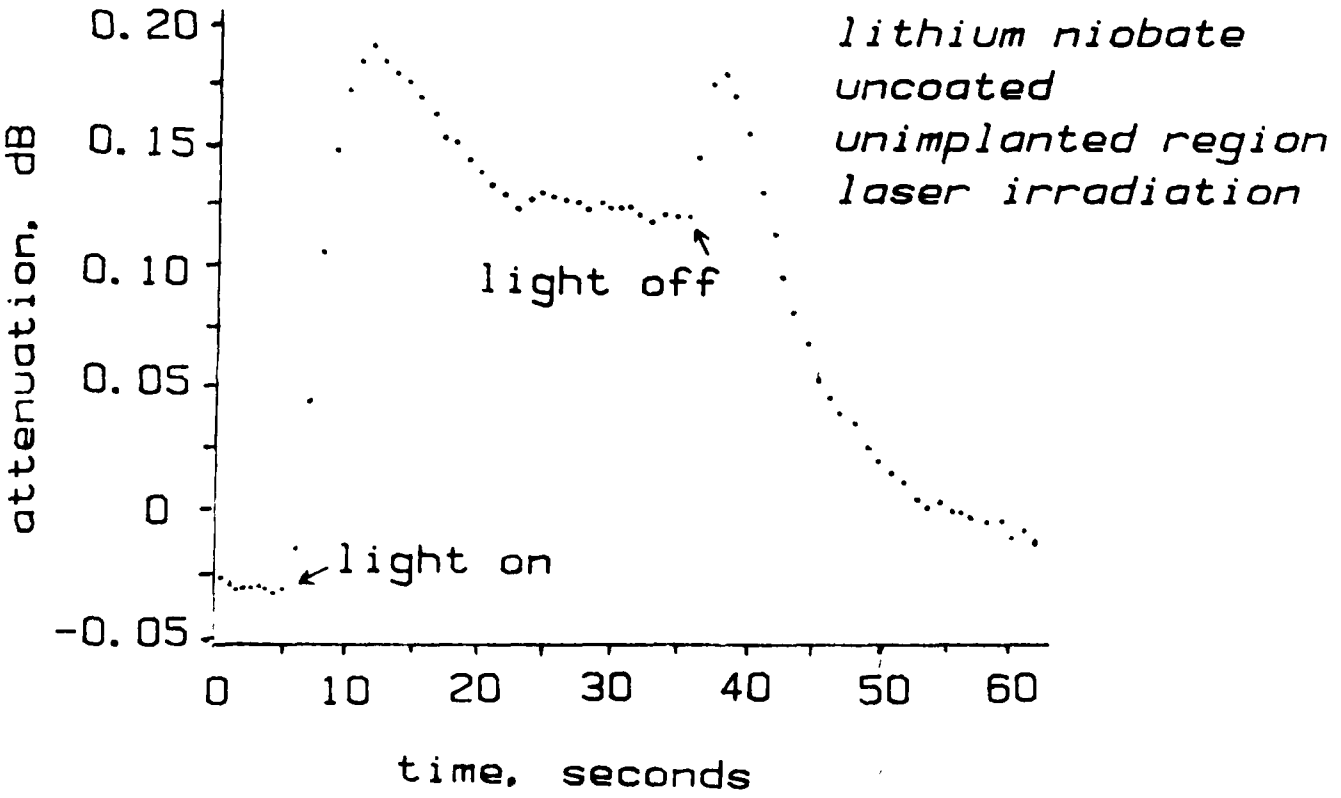

Figure 4

ACOUSTIC ATTENUATION VERSUS TIME

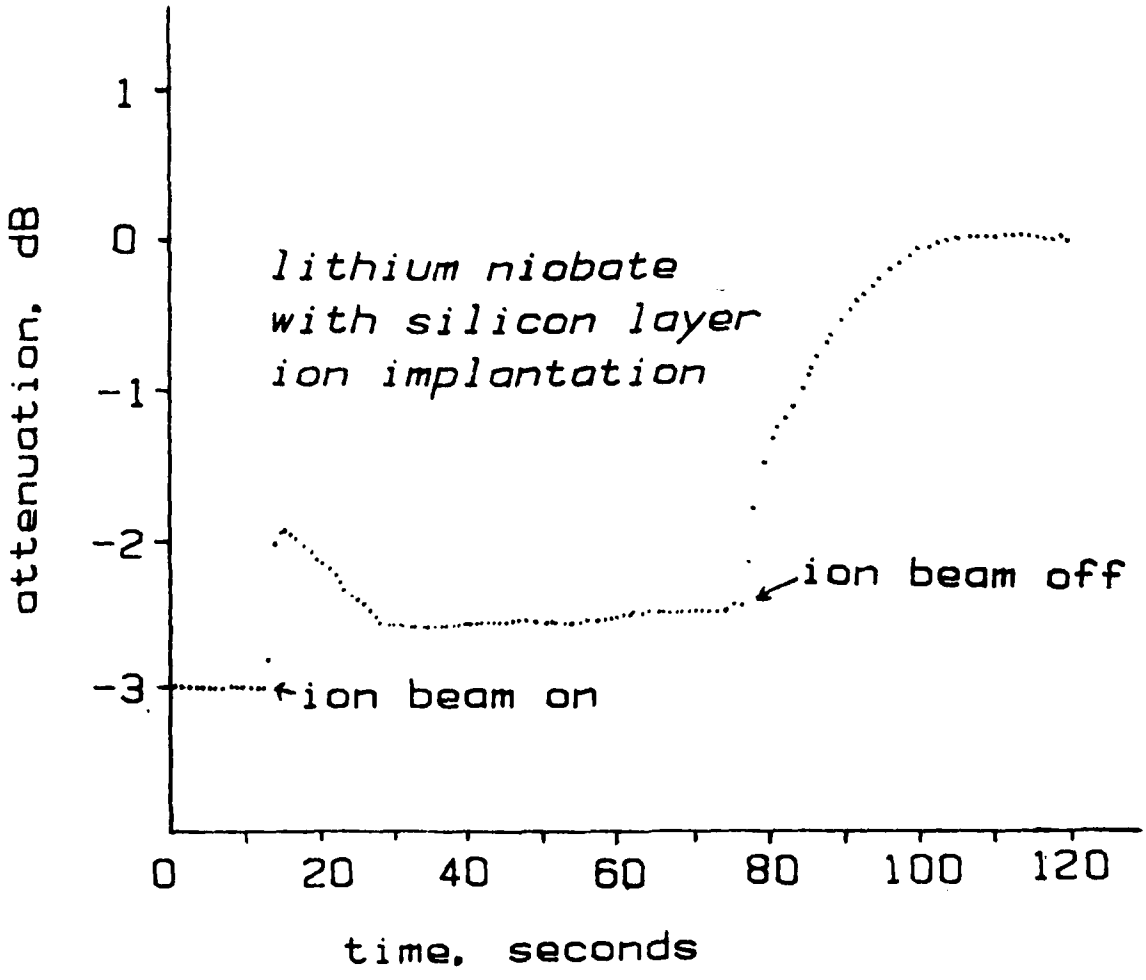

Figure 3

ACOUSTIC ATTENUATION VERSUS TIME

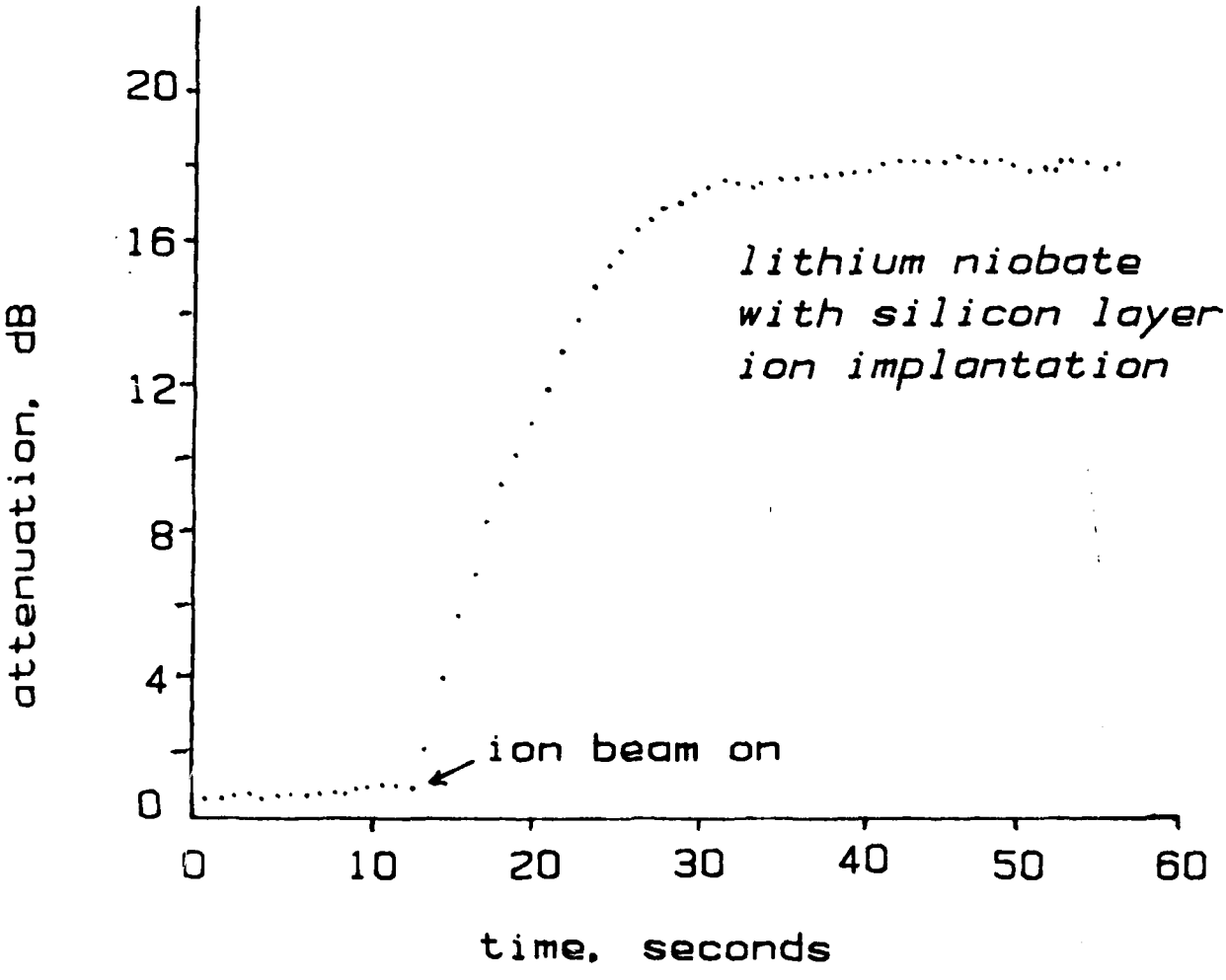

Figure 2

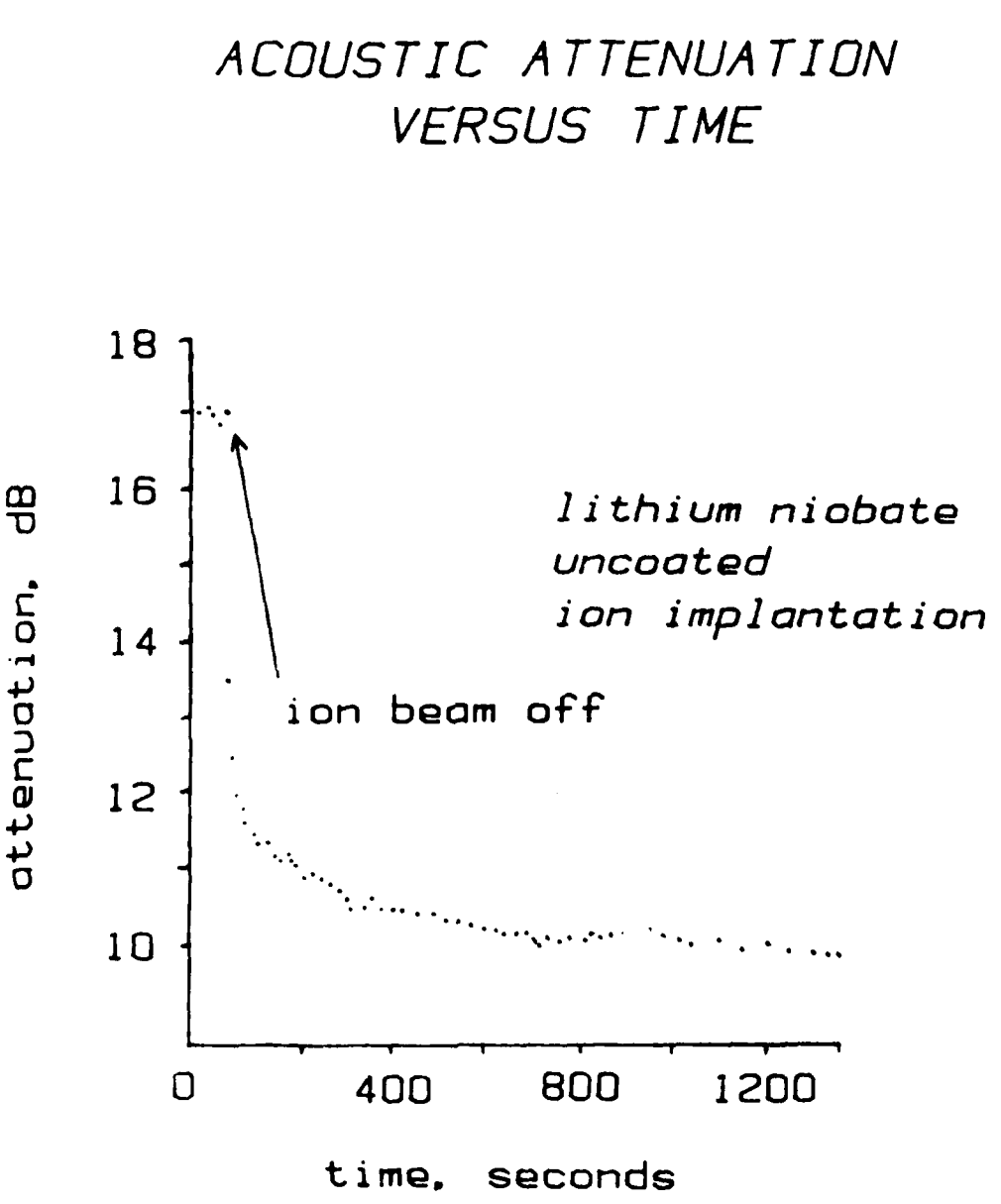
ACOUSTIC ATTENUATION
VERSUS TIME
18
16
14
12
10
attenuation, dB
lithium niobate
uncoated
ion implantation
ion beam off
0
400
800
1200
time, seconds

Figure 1b

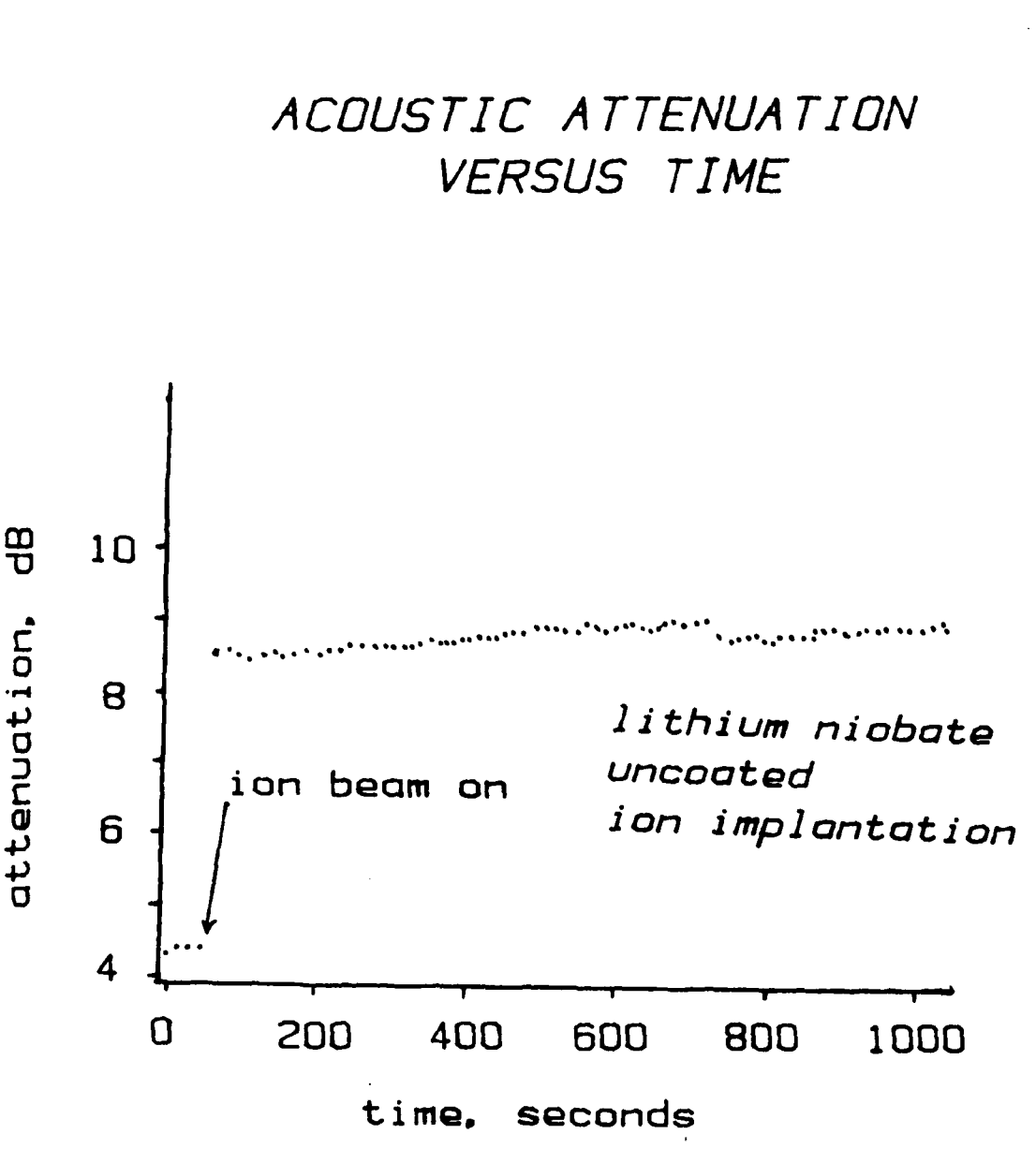
ACOUSTIC ATTENUATION
VERSUS TIME
attenuation, dB
10
8
6
4
0
200
400
600
800
1000
time, seconds
lithium niobate
uncoated
ion implantation
ion beam on

Figure 1a

by the small energy deposition near the interface of a mixing beam.

The above is a very brief summary of the results which are described more fully in the resulting publications included in Section D. Further studies of compound formation for the Cr-Si system and of the detailed structural properties of the metallic aluminum located within the silicon are in progress.

ultra-clean vacuum environment during ion implantation is being constructed and will be placed into service in a couple of months. This cleaner environment will help to reduce surface contamination during ion implantation and hence help us better characterize the changes induced in our samples. Finally, improvements in the acoustic attenuation measuring apparatus are planned: one addition will allow us to measure acoustic attenuation changes at two different frequencies simultaneously and hence we shall be better able to compare experimental results with theory.

B. Ion Beam Mixing, Profiling and High Dose Implantation into Silicon

Our initial studies focused on ion beam mixing of thin films of aluminum which were deposited upon several orientations of single crystal silicon substrates. Intermixing is demonstrated which appears to largely result from recoil mixing.[2] Nuclear resonance profiling[3] was used to study the Al depth distribution because of the effects of strong preferential sputtering upon the SIMS depth profiles. Studies of high dose implants of both Cr and Si into silicon were also carried out. These results indicate a strong dependence upon implantation conditions[4,5] and, in the case of Al, upon the silicon target orientation,[5] leading to specific conclusions about near surface distributions[4,5] for both Cr and Al in silicon.

Finally, our results upon the effect of low dose ion beam mixing upon the unit cell geometry of Nb films deposited on silicon indicate a clear dependence upon the location of the energy deposition with respect to the niobium-silicon interface. These initial studies suggest that some of the registration mismatch at the metal-silicon interface can be greatly reduced

niobate, which would tend to support the idea of electromagnetic damping of acoustic waves here. Still, there are other differences between quartz and lithium niobate, such as the thermal expansion coefficients, which might account for the relative size of the attenuation change.

Measurements of the risetime and falltime of the attenuation, as well as the size of the attenuation change, upon exposing the sample to the laser light or removing the light, indicate that the risetime/falltime constants and size of attenuation change are independent of the wavelength of the laser light. The risetime/falltime time constants appear to be independent of the absorbed power, but the size of the attenuation change depends on the light intensity, with a possible small threshold of a fraction of a watt/cm^2. (See Figure 6.)

3) Conclusions: Observations.

We have demonstrated that it is possible to perform in situ measurements of the effects of energy deposition by ion beam and laser light using surface acoustic waves as a probe. This measurement technique permits us to detect changes in the implant region during energy deposition down to a time scale of the order of one second. In addition, phenomena occurring on a shorter time scale may be studied by chopping the energy beam and using AC lock-in detection methods.

III. OTHER MEASUREMENTS:

Non-acoustic measurements, such as Rutherford Back Scattering Analysis, Electron Microprobe Analysis, and X-Ray Diffraction Analysis, will provide independent information about the damage done to the surface of our samples. Several of these measurements are now being carried out. In addition, a sample pumping station capable of placing the sample in an

the density of the material. In addition, some of these defect centers in dielectric materials may be electronically active and interact with light and the electromagnetic component of the acoustic wave propagating in a piezoelectric material. Ion beams produce sizable attenuation changes in our samples which are more or less permanent, hence we believe we are observing the production of both mechanical and electrically active defect centers during in situ ion implantation. It might be possible to separate these defect centers if we had access to S.A.W. devices on non-piezoelectric substrates, but the difficulty in fabricating such devices precludes this at present.

ii. The Generation of Charge Carriers. By contrast, laser light should produce no permanent change in the implanted samples, other than the possible bleaching of color centers from the exposure to light or a slight warming. In any event, the attenuation changes due to exposure to light appear to be fully reversible and reproducible. One tentative explanation for this reversible attenuation increase on exposure to light is the generation of mobile charge carriers or electronically active centers which in effect change the conductivity of the surface layer of the substrate. The electromagnetic component of the acoustic wave on a piezoelectric substrate is damped by this conducting layer. Independent confirmation of this effect by measuring the electrical conductivity directly has not been made and would be useful. As mentioned above, studies with non piezoelectric substrates would also be useful However, as seen in Figures 8a and 8b, the size of the attenuation change is smaller in quartz than in lithium niobate. The degree of electromagnetic coupling to mechanical waves in quartz is substantially smaller than it is in lithium

attenuation rise than the ion beam, it is believed that this effect is fairly small.

ii. Temperature Dependence of Intrinsic Attenuation.

In this model, the temperature dependence of the microscopic scattering centers (defect centers, charge carriers on a piezoelectric substrate) produces an attenuation change with rising temperature. For ion beams, most of the kinetic energy of the ion beam is deposited in a layer about 100 nm deep; similarly, the silicon film and the implant damaged (darkened) layer are of this order of thickness, hence the laser light is absorbed in a layer of this thickness as well. The conventional acoustic attenuation process is the interaction of the acoustic waves with the thermal phonons which scatter from microscopic defects and mobile charge carriers. Preliminary measurements of the intrinsic temperature dependence of the attenuation of the several samples we have studied (made by cooling and heating the samples over a temperature range of -50 C to +50 C), suggest that the dependence of the attenuation on temperature is fairly small, although this may not be true in all cases. However, because of the difference in the size of the attenuation change for ion beams and laser light of comparable intensities (discussed above) and the differences between the size of the attenuation change for quartz and lithium niobate (see Figures 8a and 8b), this appears not to be the sole machanism at work.

b. Microscopic Scattering Centers.

i. Defect Centers. The microscopic changes induced by an energetic ion impinging on a surface include microscopic mechanical damage, which scatter thermal phonons and thence acoustic waves due to inhomogeneities in

20 dB/cm. This power is to be compared to an absorbed incident light power of about 0.2 to 0.4 watts here the corresponding attenuation change is typically two to three dB/cm. Since the attenuation change is dependent on more than the incident power, mechanisms other than pure heating are responsible for attenuation changes. The second observation involves a run where the laser light was shone directly onto a S.A.W. transducer: no change in the acoustic signal was observed, even though the black wax acoustic absorbing pad directly behind the transducer appeared to have been slightly melted in the process. Thus the incident intensities being used are not sufficient to detune or otherwise affect the transducer characteristics grossly. As a result of these observations, we believe that a major portion of the attenuation changes seen during in situ energy deposition are significant effects which can be used to better understand phenomena occurring during energy deposition.

2) Some Possible Scattering Mechanisms.

a. Thermal effects

A consequence of energy deposition to the surface of the sample is the generation of a fairly complex temperature distribution, with the exposed surface being hottest and the bulk of the sample slowly warming. Several mechanisms which affect the attenuation of S.A.W.s exist and may be active here.

i. Thermal expansion. The rectangular region exposed to the laser light or ion beam will be warmed and a strain field will be produced due to thermal expansion. At present we do not have a model for attenuation produced by mechanical distortion. However, since absorbed light of intensity greater than the intensity of the ion beam produces a smaller

ACOUSTIC ATTENUATION VERSUS TIME

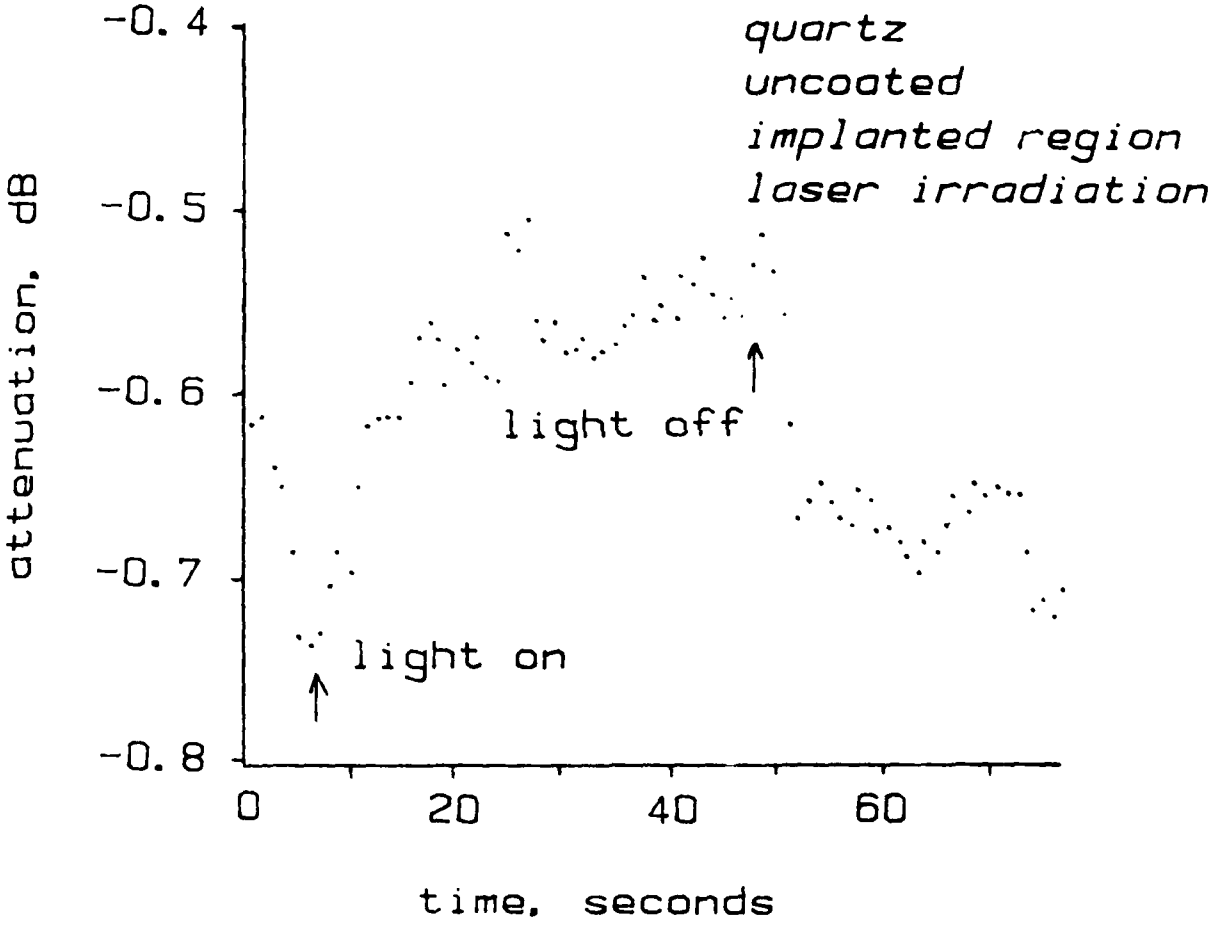

Figure 8a

ACOUSTIC ATTENUATION VERSUS TIME

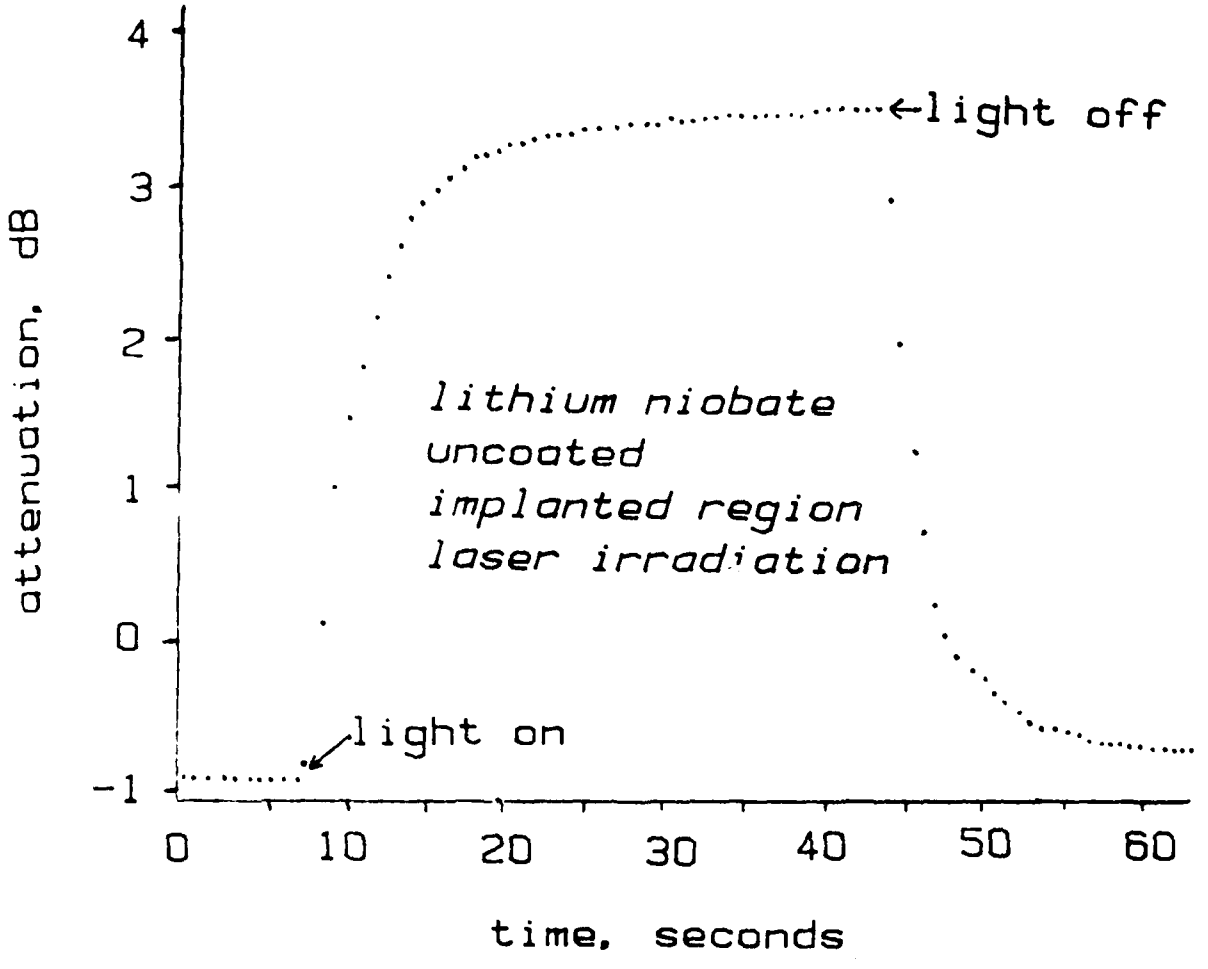

Figure 8b

C. References

1. Lipschultz, F. P., J. I. Budnick, F. A. Otter and T. W. Grudkowski. 1982. In situ study of the effects of energetic ion and laser beams on quartz and lithium niobate using surface acoustic waves. Proc. IEEE 1982 Ultrasonics Symposium:1040.

2. Namavar, F., J. I. Budnick and F. A. Otter. 1983. Chemical profiling and structural studies of ion-beam mixed aluminum on silicon. Thin Solid Films 104:31.

3. Namavar, F., J. I. Budnick, F. H. Sanchez and F. A. Otter. 1985. Nuclear resonance profiling of high dose implants of Al in Si. Nuclear Instrum. and Methods B7/8:357.

4. Namavar, F., J. I. Budnick, H. C. Hayden, F. A. Otter and V. Patarini. 1984. Study of near surface structure and composition for high dose implantation of Cr^+ into Si. Mat. Res. Soc. Symp. Proc. 27:341.

5. Namavar, F., J. I. Budnick, A. Fasihuddin, H. C. Hayden, D. M. Pease, F. A. Otter and V. Patarini. 1984. The influence of implantation conditions and target orientation in high dose implantation of Al^+ into Si. Mat. Res. Soc. Symp. Proc. 27:347.

6. Pease, D. M., F. Namavar, J. Budnick, M. Choi, J. Groeger, F. A. Otter, Y. Bruynseraede and M. Clapp. 1984. Modifications in the unit cell geometry of sputtered niobium films caused by high energy ion bombardment. Thin Solid Films 120:239.

D. Publications

1. Lipschultz, F. P., J. I. Budnick, F. A. Otter and T. W. Grudkowski. 1982. In situ study of the effects of energetic ion and laser beams on quartz and lithium niobate using surface acoustic waves. Proc. IEEE 1982 Ultrasonics Symposium:1040.

2. Namavar, F., J. I. Budnick and F. A. Otter. 1983. Chemical profiling and structural studies of ion-beam mixed aluminum on silicon. Thin Solid Films 104:31.

3. Pease, D. M., F. Namavar, J. Budnick, M. Choi, J. Groeger, F. A. Otter, Y. Bruynseraede and M. Clapp. 1984. Modifications in the unit cell geometry of sputtered niobium films caused by high energy ion bombardment. Thin Solid Films 120:239.

4. Namavar, F., J. I. Budnick, H. C. Hayden, F. A. Otter and V. Patarini. 1984. Study of near surface structure and composition for high dose implantation of Cr^+ into Si. Mat. Res. Soc. Symp. Proc. 27:341.

5. Namavar, F., J. I. Budnick, A. Fasihuddin, H. C. Hayden, D. M. Pease, F. A. Otter and V. Patarini. 1984. The influence of implantation conditions and target orientation in high dose implantation of Al^+ into Si. Mat. Res. Soc. Symp. Proc. 27:347.

6. Namavar, F., J. I. Budnick, F. H. Sanchez and F. A. Otter. 1985. Nuclear resonance profiling of high dose implants of Al in Si. Nuclear Instrum. and Methods B7/8:357.

Research Corporation

44 S. Bayles Avenue
Port Washington, New York 11050-3709
(516) 944-5120

James S. Fulleylove
Director—Evaluation

E. Invention Disclosure

January 22, 1985

Ms. Alexandra van Gelder
Assistant Vice President
The University of Connecticut
Office of the Vice President for Graduate Education and Research
Box U-133, Room 117
438 Whitney Road Extension
Storrs, CT 06268

RE: Surface Acoustic Wave Attenuation Measuring System
Lipschultz, F.
RC Disclosure No. 084-D301-84

Dear Ms. Van Gelder:

This will confirm my remarks in a telephone conversation with Dr. Frederick Lipschultz on January 11th with regard to his invention disclosure as noted above. I pointed out that in view of the apparent publication of the essential features of this invention in the proceedings following his presentation at the Ultrasonics Symposium in 1982, patenting of the invention in this country or in any of the major industrial countries would no longer be possible.

We much appreciate your giving us the opportunity to consider Dr. Lipschultz' interesting invention and hope that you or he will let us know if you should have any further questions respecting our evaluation of it.

Sincerely,

James S. Fulleylove

JSF:ll
cc: F.Lipschultz

IN SITU STUDY OF THE EFFECTS OF ENERGETIC ION AND LASER BEAMS ON QUARTZ AND LITHIUM NIOBATE USING SURFACE ACOUSTIC WAVES

F. P. Lipschultz and J. I. Budnick

Physics Department and Institute of Materials Sciences
University of Connecticut *
Storrs, CT. 06268

and

F. A. Otter and T. W. Grudkowski

United Technologies Research Center
East Hartford, CT. 06108

Abstract

Phenomena which occur at solid surfaces during ion implantation and the short term property changes which result during this exposure may be studied by sending surface acoustic waves across the implant region. Quartz and lithium niobate have been exposed to 100 keV Ar^+ ions; later these implanted regions have been studied while being exposed to intense light from an argon laser. The strength of the received surface acoustic waves is attenuated (by over 20 dB in lithium niobate) during an extended exposure to the ion beam. Upon ceasing ion bombardment there is a fast but incomplete recovery of the received acoustic signal with a time constant of the order of ten seconds. Laser light of comparable or greater intensity produces a rapid rise in attenuation of only a few dB, with a rise time of about three seconds. Upon ceasing illumination, recovery is similarly rapid but complete. From the different results produced by ion and light beams of comparable intensity, we conclude that the changes in material properties which are being observed are produced by mechanisms not entirely thermal in origin.

1. Introduction

There is considerable interest in the phenomena and material property changes associated with ion implantation. A wide variety of probes and techniques have been applied to these investigations. Since the phenomena and material property changes occur at or very close to the surface, surface acoustic waves are a useful tool for extracting information.

There have been a number of studies[1-6] of the effects of ion implantation using surface acoustic waves, but only the references by Valatka, et al., report on velocity change measurements made during the implantation process. In this paper we present the initial results of measurements of the attenuation change of 200 MHz (nominal) surface acoustic waves (SAW) during ion implantation.

2. Experiment

The quartz and lithium niobate samples were exposed to 100 keV Ar^+ ions in the ion accelerator of Prof. Howard Hayden at the University of Connecicut. The attenuation change of the SAWs (at a radio frequency of 195 MHz for quartz and 215 MHz for $LiNbO_3$) was determined by comparing the relative detected voltage height of 4 μsecond-wide, 10 kHz repetition rate pulses which were alternately switched between the implanted and unimplanted channels, both on the same sample. A PIN diode switch transferred the RF between the two channels at a 1 kHz rate, controlled by the reference oscillator of the lock-in amplifier; the voltage height of the detected RF pulses was converted to DC by the lock-in amplifier and measured by a digital voltmeter. Either the difference in pulse height voltage for the two channels or the pulse height voltage of one channel could be measured during the run. These measured voltages could be converted to attenuation changes using an earlier measurement of the pulse height voltage of the unimplanted (reference) channel alone. Tantalum masks were used to define the geometry (2 mm width by 8 mm length) and location of the implanted region, measure the incident ion current and surpress secondary electron currents.

The average Ar^+ ion current to the lithium niobate sample was estimated to be $0.27\pm.05$ uA; the average Ar^+ ion current to the quartz was estimated to be $0.75\pm.10$ uA.

Since a computer was not available to record the voltmeter readings continuously during ion implantation, it was necessary to stop the measurements to record the voltage readings stored in the voltmeter's memory from time to time, hence there are portions of the run not recorded. Because of a short which developed early during the quartz implantation, that measurement was terminated prematurely. Those portions of the lithium niobate and quartz which had been exposed to the ion beam were darkened, indicating some form of damage. It was these darkened areas which were

REPRINTED FROM
1040 — 1982 ULTRASONICS SYMPOSIUM

0090-5607/82/0000-1040 $00.75 © 1982 IEEE

exposed to intense laser beams, as reported below.

3. Experimental Results

$LiNbO_3$

Exposure of the $LiNbO_3$ to an Ar^+ ion beam of particle energy 100 keV and current density 1.7×10^{-2} A/m^2 produced an increase of attenuation with time. The response of the sample when the beam was turned on was dependent on its previous ion beam exposure. The very first exposure of the sample to the ion beam produced a gradual increase in attenuation; later after the sample had been exposed to the ion beam for a period of time and then allowed to partially recover in the absence of an ion beam, turning on the ion beam produced a rapid increase in attenuation (with a time constant of a few seconds), followed by a more gradual increase in attenuation. This trend is shown in Figure 1. Times shown are not absolute but are from the start of that particular period of the measurement. Due to experimental difficulties in establishing the beam on the sample at the beginning of the experiment, the very earliest time is not shown.

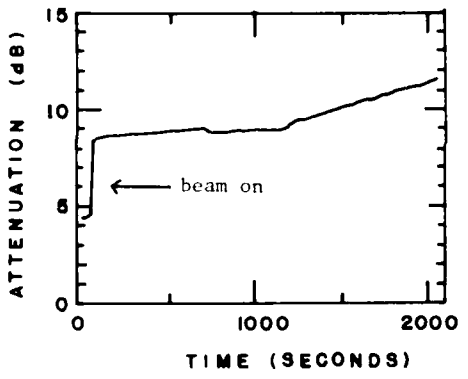

Figure 1 - Attenuation change in $LiNbO_3$ produced when the Ar^+ ion beam was turned on. The sample had been exposed to about 5.6×10^{20} Ar^+/m^2 prior to t=0 s.

Upon turning off the ion beam, there was a similar rapid but incomplete recovery in the signal amplitude in the implanted channel, as shown in Figs. 2 and 3. The time constant was on the order of ten seconds. In detail, the value of the attenuation at beam turn-off, the degree of recovery and the limiting attenuation value were dependent on the history of the sample. Our overall attenuation change per unit length (the length of the implanted acoustic channel was 8mm), of about 30 dB/cm measured in situ, for an overall fluence of 1.6×10^{21} Ar^+/m^2, appears to be significantly greater than the attenuation change reported by Larson, et al., for Ne^+ for a

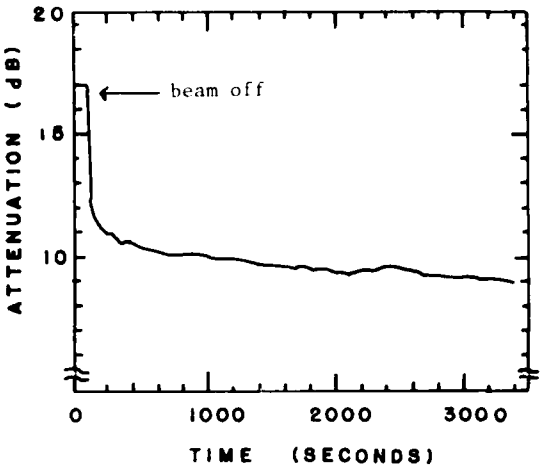

Figure 2 - Attenuation change in $LiNbO_3$ produced when the Ar^+ ion beam was turned off. The sample has been exposed to about 1.2×10^{21} Ar^+/m^2 prior to t=0 s.

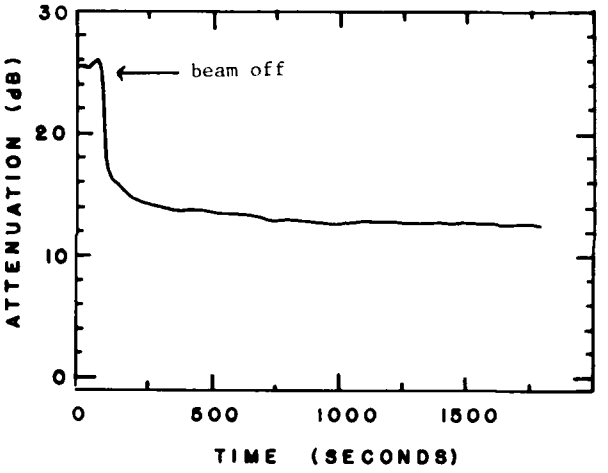

Figure 3 - Attenuation change in $LiNbO_3$ produced when the Ar^+ ion beam was turned off. The sample had been exposed to about 1.6×10^{21} Ar^+/m^2 prior to t=0 s.

corresponding fluence and SAW frequency.

Note that for an intensity of the ion beam of 1.7×10^3 W/m^2 (comparable to the intensity of sunlight), abrupt attenuation changes of 4 dB and greater, and an overall attenuation change of about 25 dB were produced. By comparison, the implanted region of the lithium niobate was exposed to several different optical wavelengths (wavelength of 515 nm, 477 and 458 nm) with absorbed intensities in the range of about 0.5 to 1.5×10^4 W/m^2, depending on the maximum power available at a given wavelength. A typical attenuation change curve (λ=515 nm, $I_{abs.}$ about 10^4 W/m^2) produced by turning the laser light on for about 40 seconds

is shown in Fig. 4. The rise and fall time of the attenuation change when the light was turned on and turned off were approximately three seconds, the attenuation change was about 4 dB, and the recovery was nearly complete. The change in attenuation was found to be proportional to the light intensity, but showed no apparent dependence on the wavelength of the light. The rise and fall times of the curve appeared to be independent of both the intensity and wavelength of the light. Recovery of the signal after the light was removed was virtually complete.

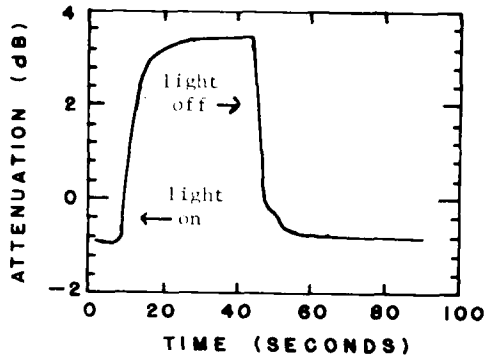

Figure 4 - Attenuation change in $LiNbO_3$ upon exposure to light from laser.

Quartz

The phenomena we observed for quartz were qualitatively similar to those for $LiNbO_3$, except that the size of the attenuation changes for ion beam exposure and laser light was smaller. Due to a short in one of the tantalum masks, the quartz implantation ended prematurely, hence the overall fluence was about 10^{21} Ar^+/m^2. However, the ion beam current was larger, being about 0.75 uA; the ion beam intensity was about 4.7×10^3 W/m^2.

The change in attenuation for quartz during ion implantation is shown in Fig. 5. Note that the sample already had been implanted briefly just prior to the time, t=0 seconds, in Fig. 5. The reason for the one dB improvement in the signal at beam turn-on is not known at this time.

The response of the implanted region of the quartz to laser light of 515 nm wavelength and an estimated absorbed intensity of about 8×10^3 W/m^2 is shown in Fig. 6. This change in attenuation for quartz was substantially less than that for lithium niobate exposed to light of the same intensity.

4. Conclusions

There are various mechanisms which we are tempted to propose to account for the attenuation changes upon exposure to the ion and light beams: heating due to energy input; density and elastic constant changes due to the damage done to the lattice by the energetic ions; mobile charge

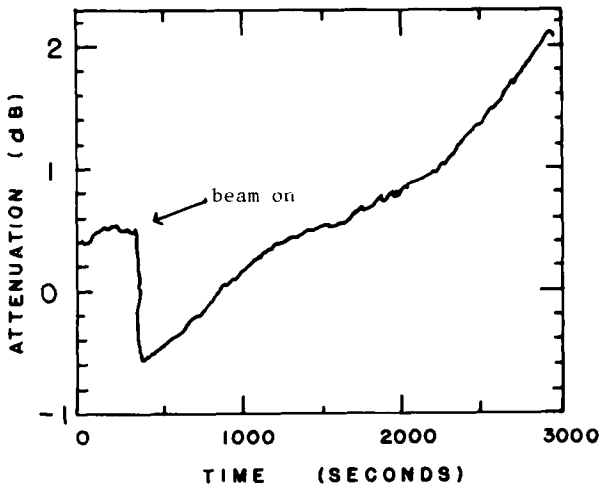

Figure 5 - Attenuation change in quartz produced when the Ar^+ ion beam was turned on. The sample had been exposed to the ion briefly prior to t=0 s.

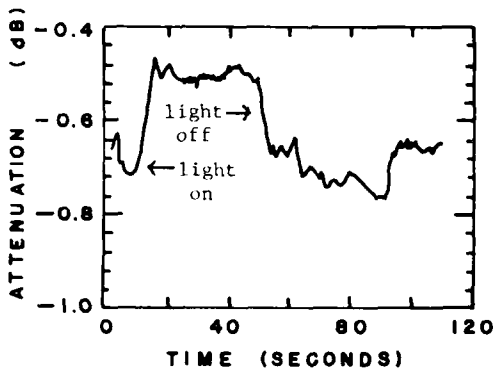

Figure 6 - Attenuation change in quartz upon exposure to light from laser.

carriers induced by the charged ion beam or the laser light. However, while there is insufficient information to adequately explain in full the observed attenuation changes, we may draw some tentative conclusions. Since the laser light produces a smaller, reversible change in the attenuation, while the ion beam produces a larger, permanent change for similar intensities, we may rule out the temperature rise as the sole cause of the attenuation changes seen. Also, the attenuation changes are larger in lithium niobate than in quartz, and since the piezoelectric coupling is larger in lithium niobate, the damping of the acoustic wave through an interaction with induced charge carriers is suggested. Further experiments to sort out these various possibile mechanisms are in progress.

5. Acknowledgements

There is inadequate space to properly acknowledge everyone who has contributed to this work. However we wish to express our appreciation to Prof. Howard Hayden, Jim Koch, and Roy Bixler for their help during the final preparation of this report.

We are grateful for the support given this work by the Office of Naval Research.

References

1. T. R. Larson, W. H. Weisenberger, and W. H. Lucke, "Effect of 80-keV Ne^+ ion implantation on acoustic surface wave attenuation in $LiNbO_3$", Appl. Phys. Lett. 22, 617 (1973).

2. P. Hartemann, P. Doussineau, and A. Levelut, "Surface-acoustic-wave velocity in ion-implanted quartz at very low temperatures", Appl. Phys. Lett. 33, 219 (1978).

3. P. Hartemann,"Influence of annealing on the surface-acoustic-wave velocity increase induced by ion implantation in quartz", J. Appl. Phys. 49, 5334 (1978).

4. P. Hartemann,"Effects of ion implantation on surface-acoustic-wave propagation", IEEE Ultrasonics Symposium (CH1482-9/79/0000-0649), pg. 649 (1979).

5. R. Y. Valatka, S. A. Jonelyunas, and L. I. Pranyavichyus,"Analysis of surface-acoustic wave propagation in a lithium niobate single crystal during H^+ and Ne^+ ion implantation", Akust. Zh. 26, 804 (1980);(Sov. Phys. Acoustics 26, 454 (1981).

6. S. Joneliunas, L. Pranyavichyus, and R. Valatka,"Surface acoustic waves in the study of ion implanted surface layers", Nuclear Instruments and Methods 182/183, 761 (1981), (North-Holland Publishing Co.).

* This work supported by the Office of Naval Research.

MODIFICATIONS IN THE UNIT CELL GEOMETRY OF SPUTTERED NIOBIUM FILMS CAUSED BY HIGH ENERGY ION BOMBARDMENT

D. M. PEASE, F. NAMAVAR, J. BUDNICK, M. CHOI AND J. GROEGER
Physics Department and Institute of Materials Science, University of Connecticut, Storrs, CT 06268 (U.S.A.)
L. A. OTTER
United Technologies Research Center, East Hartford, CT 06108 (U.S.A.)
Y. BRUYNSERAEDE
Katholieke Universiteit, Leuven (Belgium)
M. CLAPP
University of Massachusetts, Amherst, MA 01002 (U.S.A.)
(Received September 26, 1983; accepted June 19, 1984)

The effect of high energy ion bombardment on the structure of sputtered niobium films has been studied. The 1000 Å films were sputtered onto silicon substrates. The films were oriented with a [110] fiber texture and were found to have a monoclinically distorted cell characteristic of compressive stress, where the stress direction is parallel to the film surface. Bombardment with 300 keV Xe^+ ions, which for the most part did not reach the silicon interface, merely expanded the volume of the distorted as-sputtered niobium unit cell. However, bombardment with 600 keV Xe^+ ions, which have a mean range extending to the interface, relaxed the unit cell toward the configuration of a cubic geometry.

1. INTRODUCTION

Under proper conditions of pressure and other experimental parameters, sputtered films of metallic elements are often deposited in a state of compressive stress[1–4]. Several mechanisms have been suggested as contributing to such stresses in particular cases. These include argon entrapment during sputtering[2], oxygen entrapment[5,6] and "atomic peening" by high energy metal or sputter gas atoms[1,5,7]. Hoffman and Thornton[7] discovered a sudden transition from tensile to compressive stress when the ambient pressure was lowered past a threshold value; this transition pressure tends to increase with the atomic mass of the sputtered metal and may correlate with the onset of a critical energy for the atomic peening effect. Subsequently, Hoffman and Gaerttner[8] simulated the effects of atomic peening by evaporating chromium concurrently with ion bombardment. They found that the critical ion dose for a transition from tensile to compressive stress is dependent on the momentum of the bombarding species, as well as on the substrate temperature. Finally, in a recent study of stress modification in niobium by low energy ion bombardment during deposition, Cuomo *et al.*[5] separated the stress modification effects into "impurity controlled" and "structure controlled" regimes. For those films deposited at higher substrate temperatures, impurities were found to be less

0040-6090/84/$3.00

important than structural modifications of the niobium caused by ion bombardment. In this structure-controlled regime, bombardment during formation was found to change film stresses in the direction of compressive stress.

From the above discussion it may be inferred that compressive stresses can be produced by some aspect of the sputtering process which is *not* associated with the deposition of impurities but rather with a mechanical effect of the bombardment. Thus, the term atomic peening has been coined[1-5,7]. The nature of the deformation which is associated with the atomic peening process is not understood at present, and it is not the purpose of the present paper to speculate along these lines. Rather, experimental evidence is presented here which indicates that it is possible, under certain circumstances, to relieve such compressive stresses by high energy ion bombardment.

In the present study, 1000 Å films of niobium were sputtered onto silicon substrates and then subjected to bombardment with Xe^+ ions having energies of 300 and 600 keV. Samples were characterized by X-ray diffraction measurements, both with a diffractometer and with a glancing-angle Read camera. In addition, Rutherford backscattering measurements, microprobe analysis and measurements of the resistive superconducting transition temperatures T_c were carried out. Rutherford backscattering analysis and range–energy calculations indicate that the 300 keV Xe^+ ions had a mean range of about 475 Å and for the most part stopped within the niobium films, whereas range–energy calculations indicate that the 600 keV Xe^+ ions had a mean range of roughly 890 Å and caused considerable mixing with the silicon substrate. The as-deposited films, sputtered under conditions corresponding to the structure-controlled region of Cuomo *et al.*[7], were found by X-ray analysis to be under compressive stress. The 300 keV Xe ions, which were embedded in the niobium, merely expanded the volume of the unit cell without having much effect on the cell asymmetry. The 600 keV Xe ions, however, relaxed the niobium toward the configuration of relative

2. EXPERIMENTAL PROCEDURE

The films were deposited by r.f. bias sputtering in a sample chamber equipped with a liquid-nitrogen-cooled oil diffusion pump. Initial base pressure was typically 5×10^{-7} Torr in the chamber prior to sputtering. The sputtering parameters were as follows: 30 min pre-sputter of the niobium source; substrate bias of 110 V r.f.; argon pressure of 2×10^{-2} Torr; deposition rate of 3 Å s^{-1}; substrate temperature during sputtering of about 420 °C. The high substrate temperature as well as the applied bias voltage reduce the sticking coefficient of oxygen and improve film purity. The T_c value of the as-deposited film was 8.7 K, which is close to the bulk value of 9.2 K[8]. Ion bombardment and Rutherford backscattering measurements were carried out using the beam from our in-house Van de Graaff generator. The 300 keV bombardment was at a current density of 1 μA cm^{-2}, with a total dose of about 5×10^{15} ions cm^{-2}. The bombarded area was approximately 6 mm × 7 mm. The 600 keV bombardment was at a much smaller current density of 100 nA cm^{-2}, with a total dose of about 2.5×10^{15} ions cm^{-2}. The bombarded area was approximately 7 mm × 4 mm. The samples were in contact with a heat sink, and with this arrangement no detectable heating by bombardment was measured, using an IR

detector or a thermocouple, for bombardment powers much greater than those used in the present experiment. In addition, it should be mentioned that the thermal expansion mismatch stress contribution for niobium deposited onto heated silicon substrates was found to produce tensile stresses by Cuomo *et al.*[5] Thus, the compressive stresses observed in the as-deposited samples studied are due to some feature of the sputtering process rather than differential thermal contraction of film and substrate.

Electron microprobe analysis was carried out for oxygen, carbon, argon, niobium and xenon. A 10 kV electron beam potential was used with an incident current of 1×10^{-7} A. The sample tilt was 20° with respect to the horizontal, with an X-ray take-off angle of 45°. The electron optical column ran at a pressure of 4×10^{-8} Torr with a differentially pumped specimen chamber pressure of 1×10^{-6} Torr. X-ray peak data were taken with a wavelength-dispersive spectrometer with the electron beam rastering over a rectangular pattern measuring 150 μm × 100 μm. The peak intensities were referred to pure standards where possible. However, in the case of oxygen, magnesium oxide was used, and for xenon and argon peaks reference values were interpolated from measurements taken on adjacent elements. The intensity of the Si Kα X-ray line was also measured, for these samples as well as for a 2000 Å niobium film on silicon, in order to obtain information on the attenuation of the electron beam by the niobium films.

Our quantitative analysis computer program for analyzing microprobe data is intended for use with bulk samples and leads to errors in the present application. The attenuation of the O Kα and C Kα lines is sufficiently large in niobium that a 1000 Å niobium film is effectively a bulk sample as far as these elements are concerned. Since the Nb Lα line is much less attenuated than the O Kα or C Kα lines, 1000 Å of niobium does yield a weaker niobium signal than would a bulk sample for the electron bombardment conditions used. Thus, the bulk analysis routine tends to overestimate the concentration of carbon and oxygen relative to niobium for a 1000 Å niobium film. In addition, as pointed out by Cuomo *et al.*[5], oxygen and carbon concentrations may be largely surface oxides and surface carbon so that, for this reason as well, the values given should be regarded as upper limits on the concentration within the body of the films. The oxygen and carbon concentrations determined by microprobe analyses of the bombarded specimens, using the bulk sample analysis routine, were approximately equivalent to atomic fractions of 0.1 for oxygen and 0.17 for carbon. The oxygen value is comparable with or less than that obtained by Cuomo *et al.*[5], although the measured carbon concentration is higher; as argued above, these microprobe values tend to overestimate the concentration of these impurities within the film. Although quantitative analysis was not carried out for the as-deposited specimen, a comparison of X-ray intensities indicates that the oxygen and carbon impurities in the as-deposited specimen were somewhat lower in concentration than in the bombarded samples. Additional evidence that the bulk volume of the films contains less oxygen than indicated by the microprobe results may be found from the measured T_c value of the as-deposited sample, since T_c is depressed by about 0.9 K per atomic per cent of oxygen[9]. The measured T_c value of 8.7 K, which is lower than the bulk T_c value by 0.6 K, is thus consistent with an oxygen concentration of only 0.7 at.% in the as-deposited film. For bulk niobium, addition of 1.0 at.% O expands the lattice constant by 0.005 Å [9], a result which is not

inconsistent with X-ray diffraction results obtained in the present work. Finally, analysis of noble gas inclusions reveals that argon was entrapped in the samples at a concentration of a few tenths of an atomic per cent. The xenon distribution in the 300 keV bombarded sample is essentially uniform and corresponds to about twice the average xenon concentration in the 600 keV sample, in agreement with the calculated total xenon dose. The xenon distribution in the 600 keV sample varies by about a factor of 2 across the longer sample dimension. Since the X-ray diffraction data discussed later represent an average sampling of the bombarded region, the details of the xenon distribution do not affect the conclusions which follow.

X-ray measurements were obtained using a diffractometer and a Read thin film camera[10]. The diffractometer was outfitted with a copper anode X-ray tube and a graphite monochromator. The angular accuracy of the diffractometer was checked using the (331) reflection of a silicon standard. The angular error is quite negligible compared with the observed peak shifts between the as-deposited, the 300 keV bombarded and the 600 keV bombarded samples. Most of the error in locating the positions of the rather broad niobium peaks resides in uncertainties in determining the precise angular position of peak intensity; the observed peak shifts due to stress effects, however, are larger than all errors encountered in the diffractometer measurement. All Read camera exposures were carried out using a 0.25 mm beam collimator, glancing angles of 10° or 20° and either a copper, cobalt or iron target X-ray tube. Read camera photographs of niobium thin films were measured using an optical comparator. Whereas most previous investigators of stresses in sputtered films have measured stresses by means of the deformation of thin substrates[5-8], in the present study the deformation of the unit cell is measured. For this purpose the combination of Read camera and diffractometer results was used to yield information about the interplanar spacing of diffraction planes both parallel and not parallel to the film surface.

3. RESULTS

Read camera photographs of all samples were consistent with a [110] fiber texture for the niobium films, with the fiber axis almost exactly normal to the film surface. All arcs were indexed and related to interplanar angles using established solutions of the Read camera cylindrical diffraction geometry[11]. There is a faint arc in the (110) ring which indicates a slight admixture of some orientation other than [110]. Diffractometer scans of all three samples were taken to a value for twice the Bragg angle of 85°. These scans revealed niobium (110) and (220) reflections, consistent with the [110] fiber texture revealed by the Read camera. It will be convenient, for purposes of discussion to follow, to define the *b* axis of the niobium unit cell to be parallel to the film surface, as is indicated in Fig. 1. Thus, the set of lowest index planes parallel to the film surface will from now on be designated (101) rather than (110).

In addition to the niobium (101) and (202) reflections, one relatively weak additional peak was detected in the diffractometer scans of all the samples. This peak has the appearance of a Bragg angle satellite to the niobium (202) reflection and occurs at a value for twice the Bragg angle of 83.5°. The area under the satellite peak is enhanced in the bombarded samples, and the peak might have escaped detection for

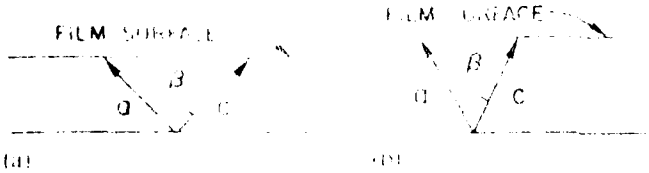

(a) (b)

Fig. 1. Schematic illustration of the niobium unit cell, oriented with (101) planes and the *b* axis parallel to the film surface (a) cubic cell, (b) monoclinic distortion caused by compressive stress.

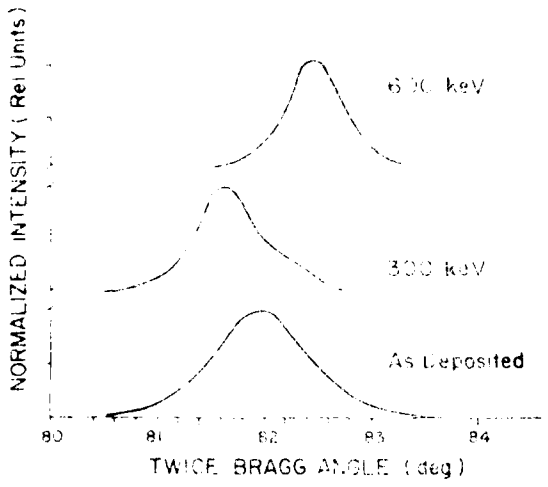

Fig. 2. Intensities of the (202) niobium reflection for samples denoted 600 keV bombarded, 300 keV bombarded and as deposited. Peak heights are normalized to the same height.

the case of the as-deposited film if the bombarded samples were not available for comparison. The source of the satellite peak has not as yet been identified. Since the emphasis of the present paper is on the effect of bombardment on the majority niobium phase the rest of the discussion will concentrate on the main niobium peaks in the X-ray pattern.

Diffractometer scans of the main (202) reflection corresponding to as-deposited niobium, 300 keV bombarded niobium and 600 keV bombarded niobium are shown in Fig. 2. In the figure, the peaks are all normalized to the same maximum intensity. The value for twice the Bragg angle which would correspond to unstressed pure niobium is 82.7°. This value corresponds more closely to the position of the bombarded 600 keV peak than to the (202) peaks in the other samples. In addition, the width of the 600 keV (202) peak is less than the width of the (202) peak for the as-deposited film. The maximum intensity of the 300 keV peak is significantly less than that of the other peaks in the non-normalized data.

Figure 3 shows a Rutherford backscattering spectrum of the 300 keV bombarded specimen compared with an unimplanted sample. The xenon profile indicates that the penetration depth of xenon is about 400 Å, which agrees well with theoretical range-energy calculations of the mean xenon penetration depth. For the 600 keV bombarded sample, range energy calculations indicate that the mean range of the xenon ions is about 890 Å. A clear xenon profile is not expected in this case, partially because the signal from xenon ions at depths beyond 550 Å will superimpose on the niobium signal. An increased spread of the xenon distribution for the 600 keV case, is also of importance in this regard. The Rutherford backscattering spectrum of the 600 keV sample is shown in Fig. 4. Further analysis

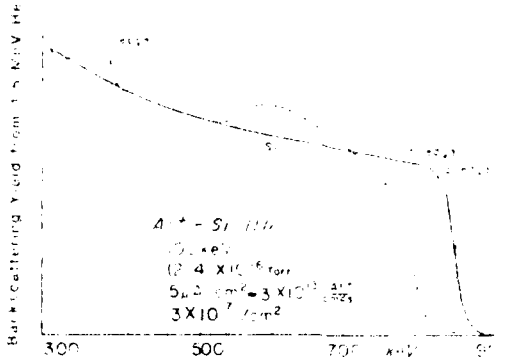

Fig. 3: RBS spectrum of Al implanted into Si (111) (FDPV).

Fig. 4 demonstrates RBS spectra of implanted Al in Si (100) in a trapped diffusion pumped system with a dose rate of 3×10^{14} ions/cm^2 sec and different doses. These data suggest that as the dose of implantation increases, the Al concentration profile shifts to a greater depth. For doses of 2×10^{18} ions/cm^2, Al penetrates to a depth which is almost twice that of the projected range. Two x-ray lines which correspond to (111) and (200) Al reflections were observed at intensities expected for polycrystalline aluminum.

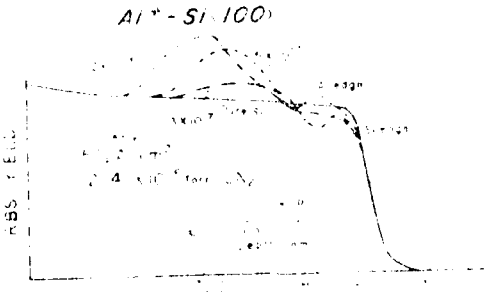

Fig. 4: RBS spectra of implanted Al into Si (100) (DPV).

Fig. 5 demonstrates RBS results of Al implanted with 200 keV energy, a dose of 1×10^{18} ions/cm^2 and a dose rate of 6.2×10^{13} and 3.1×10^{14} ions/cm^2 sec into Si (100) and Si (100) targets in an HV system operating at $(2 \pm 1) \times 10^{-8}$ Torr. As is shown, Al [illegible] much deeper than the projected range. A [illegible] concentration of Al could be [illegible] into Si (111) [illegible] Al [illegible] with [illegible] Al [illegible] were observed for all four samples while RBS results are [illegible] in Fig. 5.

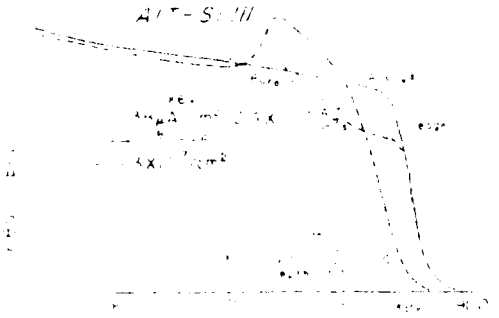

Fig. 1: RBS spectra of 1.5 MeV He^+ for Al implanted Si (111) samples (TIPV).

been observed for all Al implanted samples into Si (111) substrates with dose ranging from 3×10^{16} to 10×10^{17} ions/cm^2 and at a dose rate of 2.4×10^{14} ions/cm^2 sec. However, no x-ray peaks due to reflections from other planes could be observed in our diffractometer, in contrast to the Al implanted Si (100) samples which do not show such preferential orientation.

The RBS spectra for a dose rate of 3.3×10^{13} ions/cm^2 sec into Si (111) (TIPV) at a dose of 3×10^{17} ions/cm^2 is shown in Fig. 3. A thin carbon film on the surface is observed. No elemental Al peaks could be observed by x-ray diffractometry for the low dose rate implanted samples.

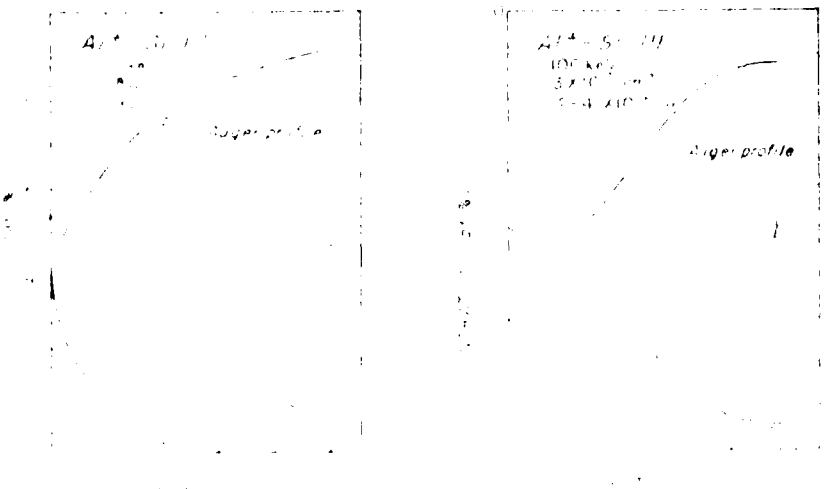

Fig. 2: Depth profiles by AES of
Fig. 3: (a)
(b)

Since the production of an oxygen-free Al-Si interface is normally very difficult, we proceeded to prepare Al-Si mixtures by direct high dose implantation of Al into silicon. Our interest in this work was enhanced because of recent stimulating work on metal-semiconductor eutectic systems [3-6]. For some of the metal-semiconductor eutectic systems such as Au-Si and Au-Ge, metastable phases have been produced by splat cooling, laser and ion beam experiments [3, 7].

Therefore, it seemed very interesting to study by high dose implantation techniques the possible existence of metastable phases in the Al-Si system and to determine the dependency of formation of such a phase upon contaminating elements such as oxygen. Here, we report preliminary results of the first part of this study, namely, the influence of implantation conditions and target orientation for high dose implantation of Al into Si and the results of studies by RBS, x-ray diffractometry, and AES. We are also in the process of applying nuclear resonance profiling (NRP) using the $^{27}Al\ (p,\gamma)\ ^{28}Si$ reaction in order to obtain additional information on the depth of profile for Al.

EXPERIMENTAL PROCEDURES

Polished single crystals of Si with (111) and (100) orientations were implanted with 150 keV Al^+ ions by means of the high current implanter of The University of Connecticut. During implantation three parameters were varied:

(i) dose, ranging from 1×10^{17} to 2×10^{18} ions/cm^2
(ii) dose rate, ranging from 3×10^{13} to 3×10^{14} ions/cm^2 sec
(iii) vacuum conditions, diffusion pumped vacuum system with and without liquid nitrogen trap $(2-4) \times 10^{-6}$ Torr and an ultra high vacuum (UHV) system $(2-4) \times 10^{-8}$ Torr

During implantation and RBS, samples were tilted to 10° from the normal incidence of the ion beam and were fastened to the heat sink with conductive materials (silver paint). The temperature of some high dose 10^{18} implantations was monitored and no rise in target temperature was observed.

EXPERIMENTAL RESULTS

Fig. 1 demonstrates the RBS results for Al implanted Si (111) samples in the untrapped diffusion pumped system (DPVV), with 150 keV energy and doses of 1 and 10×10^{17} ions/cm^2 and a dose rate of 2.5×10^{14} ions/cm^2 sec. As is shown for the sample implanted with a dose of 3×10^{17} ions/cm^2, there is a substantial reduction in the backscattered signal for both Al and Si at 2,500Å. However, Si constitutes about 2/3 of the surface atoms.

A more reduction of scattering signal was observed for doses such as 5×10^{17} ions/cm^2 as compared with ones with a dose of 3×10^{17} ions/cm^2. It appears that the backscattered signal from the Si surface is reduced as the implant dose is increased. Eventually, at a dose of 1×10^{18} ions/cm^2, there is a predominance of Al for depths less than 2,500Å.

Auger depth profiles by Auger electron spectroscopy of samples similar to those in Fig. 1 have been carried out and are demonstrated in Fig. 2. From these data, the formation of a thin Al oxide layer at the Al surface is observed, which was suggested by RBS at a dose of 3×10^{18} ions/cm^2 is confirmed. Although we cannot accurately estimate the effect of preferential sputtering on the AES data, the RBS and AES results are in agreement. The dose samples were studied by means of an x-ray diffractometer. By this means, a pronounced (111) Si reflection peak has

THE INFLUENCE OF IMPLANTATION CONDITIONS AND TARGET ORIENTATION IN HIGH DOSE IMPLANTATION OF Al^+ INTO Si

F. NAMAVAR,* J. L. BEEMAN,* A. FASIHUDDIN,* T. C. HAYDEN,* D. A. PEASE,* R. L. OTTEN,** AND T. PATAJINI** *The University of Connecticut, Storrs, CT 06268; **United Technologies Research Center, East Hartford, CT 06108

ABSTRACT

We report the preliminary results of a study to determine the dependence of the near surface composition and structure on total dose, dose rate, vacuum condition and substrate orientation for Al implantation into Si (111) and Si (100) with doses up to 2×10^{18} ions/cm^2. Our studies include the results of Rutherford Back Scattering (RBS), Auger Electron Spectroscopy (AES) and x-ray diffraction measurements on samples implanted with a 100 keV energy in a diffusion pumped vacuum (DPV) system (10^{-6} Torr) with and without a LN_2 trap and in an ultra high vacuum (UHV) system ($2-4) \times 10^{-8}$ Torr.

Results of high dose rate (50 $\mu A/cm^2$) implantation into Si (111) in an untrapped DPV system indicate that Al segregates with a preferred (111) orientation. For a dose of 1×10^{18} ions/cm^2 the surface is Al-rich to a depth of 2500Å while for lower doses the surface is silicon-rich. A carbon build-up occurred for samples prepared by low dose rate (5 $\mu A/cm^2$) implantation. However, no Al segregation could be observed for doses of less than 10^{18} ions/cm^2. A similar behavior has been observed for Si (100) except that Al segregation occurs with a polycrystalline structure. Moreover, the segregated Al is present at depths greater than the projected range.

When implantation was carried out in a DPV system with a LN_2 trap, no carbon peaks could be observed by RBS regardless of the dose rate. For these conditions, as well as for the implantation of Al in an UHV system, we find Al segregation with a polycrystalline structure independent of the ion dose rates and target orientations we used. Al is observed at a depth greater by a factor of $\sqrt{2}$ than the expected value from the R_p calculations. The Al depth penetration increases with the dose of implantation.

INTRODUCTION

We have recently shown [1] that, under certain conditions, the implantation of ions through the insertion of oxygen in Al thin films on Si substrates can produce an Al [illegible] which is uniform in texture. Segregation was observed for [illegible] at room temperature annealing. For a number of experiments [illegible] of Al Si alloy layers was stable under heat treatments [illegible] this temperature a thin film of Al is formed [illegible]. We have been very interested in understanding the [illegible] and in determining the dependence of stability [illegible] oversized impurities such as oxygen and [illegible]

implantation causes Cr atoms to move toward the interface (as well as deeper) and/or the C-Si/Si interface also moves to the Cr-rich region because the surface Si is consumed by the Si-C reaction as well as by sputtering.

At certain doses which obviously should be less than 1×10^{18} ions/cm^2, a large number of Cr atoms will reach the interface and come in contact with the carbon present in the C and Si region. One would expect that further implantation should initiate a reaction between Cr and carbon. Very recently it was reported that chromium carbide was formed by implantation of Cr^+ into the CrFe system [9]. In addition, so-called vacuum carbonization [4] is cited to occur for pure Fe, Ni and Ta by a variety of ions such as Ti^+, Ta^+ and Cr^+. Our RBS and AES indicate that carbon occurs more readily at a surface rich in silicon than for one rich in Cr.

However, we believe that, if in both high and low dose rate implantation a uniform C-Si layer is created, then there should be no difference in Cr concentration or in retention for a relatively high dose implantation because sputtering is a surface phenomenon. On the other hand, if islands of C-Si are formed, we believe that a reduction of sputtering or an increase in retention of implanted atoms will depend on the surface concentration of these islands. More islands are probably created during low dose rate implantation because of a longer implantation time. The low dose rate implantation time was about 50 times that of the high dose rate implantation (Fig. 6).

Because of the lack of required resolution RBS and AES techniques cannot be applied in order to verify the lateral uniformity of implanted surfaces. Therefore, we have studied samples implanted with doses of 3 and 5×10^{17} ions/cm^2 by scanning electron microscopy. SEM micrographs indicate the presence of light spots which could be associated with exposed Si surfaces.

†Supported by the Office of Naval Research.

REFERENCES

1. Z.L. Liau and J.W. Mayer, J. Vac. Sci. Technol. 15(5) 1-29 (1978).
2. E. Arminen, A. Fontell, and V.K. Lindroos, Phys. Stat. Sol. (a) 4 663 (1971).
3. R. Kelly and J.B. Sanders, Surface Science 57 143 (1976).
4. I.L. Singer, J. Vac. Sci. Technol. A1(2) 419 (1983).
5. W.K. Chu, J.W. Mayer and M.A. Nicolet, Backscattering Spectroscopy (Academic Press, New York 1978).
6. M. Hansen, Constitution of Binary Alloys (McGraw-Hill, New York 1958).
7. F. Schulz and K. Wittmaack, Radiation Effects 29 31 (1976).
8. P. Blank, K. Wittmaack and F. Schulz, Nuclear Instruments and Methods 132 387 (1976).
9. W.K. Chan, C.R. Clayton, R.G. Allas, C.R. Cossett and L.A. Hirvonen, Nuclear Instruments and Methods 209/210 857 (1983).

ACKNOWLEDGMENTS

We are very grateful to Professor Quentin Kessel for his help with the Van de Graaff accelerator, to Professor D. L. Potter for allowing us to use his ultra high vacuum implantation chamber and to M. Ahmed for his assistance during implantation. In addition, we would like to thank R. Koser, P. Clapis, John Giannopoulous and C. H. Poel for their technical assistance.

Assuming the validity of this model, twice the absolute value of the slope of the fitted line gives the sputtering factor. We can then conclude that the sputtering factor for a normal incident Cr^+ beam with 100 keV energy and a dose rate of 6.2×10^{13} ions/cm^2 sec is about S = 1.06. This value can be considered as the lowest limit for the sputtering factor, if range shortening [8] due to previously implanted atoms influences the range distribution of implanted ions.

In Fig. 1 the profile of Cr for implantation with a dose of 3×10^{17} ions/cm^2 is relatively flat. Fig. 3 indicates that, although no change in R_p can be observed, the value of straggling increases. Considering Fig. 2, one can realize that the Cr concentration is comparable with $CrSi_2$.

Fig. 2 shows that by increasing the system pressure by two orders of magnitude, concentration and retention of implanted atoms increases by a factor of 2 and 3 respectively. The RBS results shown in Fig. 4 demonstrate that an increase in the concentration and retention of Cr atoms is always accompanied by the presence of a carbon or an oxygen peak. These peaks indicate that surface of these samples possesses large amounts of carbon or oxygen depending on the surface composition which in turn is controlled by the total dose. Fig. 4 demonstrates in addition that the near surface region of samples implanted with doses of 3 and 5×10^{17} ions consists predominantly of Si atoms. Moreover, about 1.1×10^{17} and 1.4×10^{17} carbons/cm^2 are present in the surface region as a result of implantation of 3 and 5×10^{17} ions/cm^2 respectively. On the other hand, for implantation with a total dose of 1×10^{18} ions/cm^2, the carbon peak has disappeared and a small oxygen peak emerges which corresponds to about 3.3×10^{16} oxygens/cm^2.

Two mechanisms can be responsible for the introduction of oxygen or carbon into the surface sample: (i) recoil implantation of elements of adsorbed residual gas and/or (ii) enhancement of the chemical reaction of surface atoms with the element, of adsorbed residual gas as a result of ion implantation. It is well known that during implantation the surface impurity is recoil-implanted into the target (3). However, as can be seen from the result (Fig. 4), if recoil implantation is responsible for the introduction of oxygen and carbon in our samples, one should expect both oxygen and carbon to be present in large quantities at the same time.

On the other hand, Fig. 4 suggests that when surface targets are predominantly constituted of Si atoms, a carbon build-up occurs. However, when the dose of implantation was increased to 1×10^{18} ions/cm^2, mostly Cr atoms reached the surface and the carbon peak disappeared while an oxygen peak appeared. AES results of the above sample at a depth of 50Å clearly support the conclusion derived from RBS data.

At this time we believe that the mechanisms involved in this process are chemical in nature because the association of oxygen or carbon occur preferentially and depend upon surface composition. Besides from our results, it seems that during implant there is a strong affinity between Si and C as well as between Cr and O. This fact fines the presence of carbon or oxygen patterns.

A potential transformation of implanted samples from a carbon rich surface (with a dose of 5×10^{17} ions/cm^2) to an oxygen rich surface (with a dose of 1×10^{18} ions/cm^2) merits serious consideration. By implanting Cr with a dose of 5×10^{17} ions/cm^2 a surface layer rich in C and Si is observed (see Figs. 4 and 5a). At this stage of implantation very few Cr atoms are present on the C-Si surface. Indeed, the latter can be verified by the experimental results shown in Fig. 5. Further

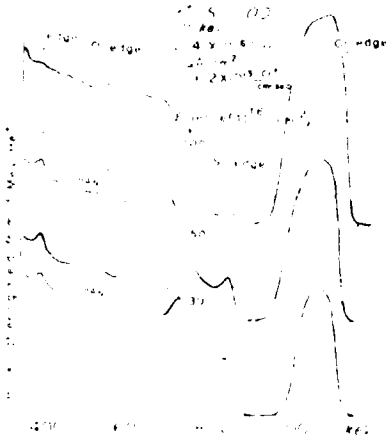

FIG. 4: RBS spectra of Cr implanted with 100 keV energy and a dose rate of 6.2×10^{13} ions/cm^2 into Si in a DPV system (2-4) x 10^{-6} Torr.

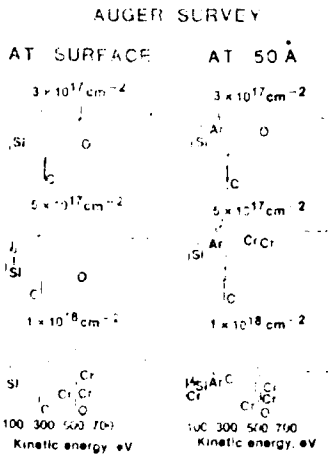

FIG. 5: AES data for the surface and for a depth of 50 Å for those samples whose RBS data are shown in Fig. 4.

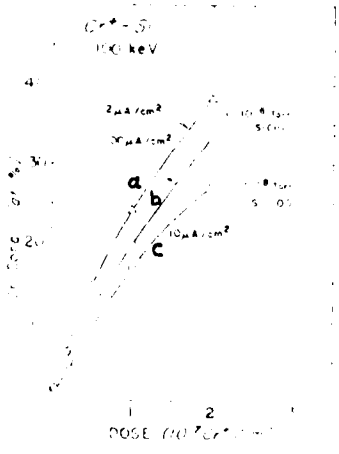

FIG. 6: Cr concentration curve versus implantation dose.

of an implanted atom does not change by subsequent implantation, and (iv) enhanced diffusion does not occur. During implantation, as a result of surface sputtering, the depth profile of the implanted atoms moves toward the instantaneous surface where the amount of the shift is equal to half the thickness of sputtered layers for symmetrical range distribution [7].

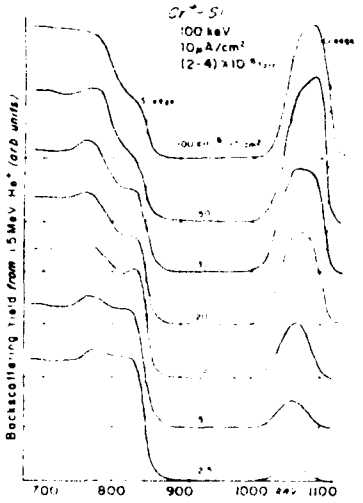

FIG. 1: RBS spectra of 1.5 MeV He^+ for implanted Cr^+ into Si with 100 keV energy.

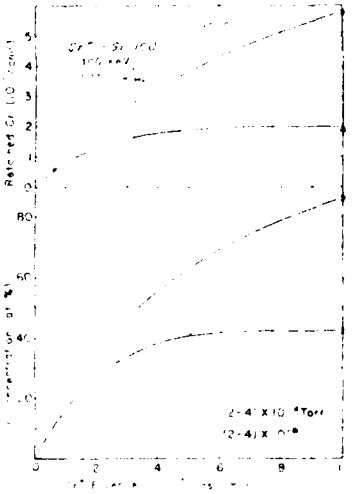

FIG. 2: Concentration and retention curves for implanted Cr^+ into Si
▲ : Implanted in UHV system
● : Implanted in DPV system

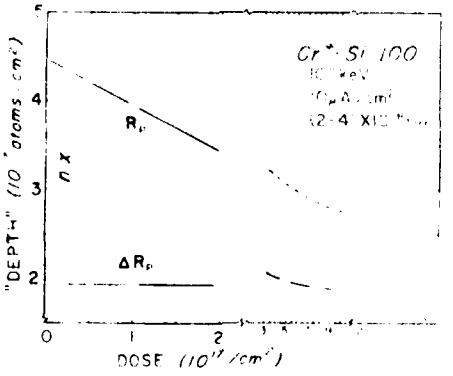

FIG. 3: Projected range (R_p) and straggling (ΔR_p) determined from the data of Fig. 1 (UHV).

the surface (Fig. 1), and the concentration is less than 27% (Fig. 2). The Cr-Si phase diagram [6] does not suggest the existence of any compounds with Cr concentration of $\lesssim$27%. It therefore seems possible that the zero order approximation model [7] can be applied to the first four data points. In zero order approximation one assumes that: (i) range distribution of implanted ions is not influenced by atoms previously introduced, (ii) surface sputtering is defined by a constant factor, (iii) the rest position

(2) a beneficial effect, i.,e., the production of a protective layer from sputtering. Indeed, because of this protective layer, we have been able to achieve a very high concentration (86%) of Cr for the Cr-Si system.

EXPERIMENTAL PROCEDURES

Polished single crystals of Si with (111) and (100) orientations were implanted with energetic Cr^+ ions ranging from 40 to 160 keV by means of the high current implanter of The University of Connecticut. During implantation three parameters were varied:

(i) dose, ranging from 1×10^{16} to 2×10^{18} ions/cm^2
(ii) dose rate, ranging from 5×10^{12} to 3×10^{14} ions/cm^2 sec
(iii) vacuum conditions, DPV system with and without liquid nitrogen trap $(2-4) \times 10^{-6}$ Torr and an UHV system $(2-4) \times 10^{-8}$ Torr

During implantation and RBS, samples were tilted to 10° from the normal incidence of ion beam and were fastened to the heat sink with conducting materials (silver paint). The temperature of some high dose rate implantations was monitored and no rise in target temperature was observed.

EXPERIMENTAL RESULTS

Fig. 1 demonstrates the RBS spectra of implanted Cr into Si(100) with 100 keV energy and a dose rate of 6.2×10^{13} ions/cm^2 sec and doses ranging from 2.5×10^{16} to 10^{18} ions/cm^2 in a UHV system operating at a pressure of about $(2-4) \times 10^{-8}$ Torr. Cr concentration at the maximum for each individual implanted sample was calculated [5] and is shown versus dose of implantation in Fig. 2. It is clear that a steady state concentration (42%) was achieved for a dose of about 5×10^{17} ions/cm^2. Implantations with higher doses do not result in higher Cr concentrations.

Fig. 3 demonstrates the projected range (R_p) and straggle (ΔR_p) determined from the RBS data of Fig. 1 along with estimates of stopping cross sections for He^+ in Cr-Si.

Fig. 4 shows RBS spectra of Cr implanted with 100 keV energy and a dose rate of 6.2×10^{13} ions/cm^2 sec into a Si(100) target, in a DPV system operating at a pressure of $(2-4) \times 10^{-6}$ Torr. Cr concentration as well as Cr retention for implantation in a chamber with a pressure in the order of 10^{-6} Torr are plotted in Fig. 2.

Fig. 5 shows AES data at the surface and at a depth of 50Å for those samples whose RBS are shown in Fig. 4. RBS and AES results are in very good agreement.

Curves a and b of Fig. 6 demonstrate the Cr concentration curves versus implantation for samples prepared in a DPV system operating at pressures of about 10^{-6} Torr and a dose rate of 6.2×10^{14} and 1×10^{13} ions/cm^2 sec respectively. Curve c in Fig. 6 is plotted for purposes of comparison and demonstrates the Cr concentration for implantation in a UHV system. From these results it is obvious that when implantation is carried out at a pressure of about 10^{-6} Torr a higher concentration of implanted Cr can be achieved for a low dose rate implantation.

DISCUSSION AND CONCLUSION

An examination of the first four data points of Fig. 2 suggests that depth decreases linearly with dose. For these lower doses, Cr lies beneath

STUDY† OF NEAR SURFACE STRUCTURE AND COMPOSITION FOR HIGH DOSE IMPLANTATION OF Cr^+ INTO Si

F. NAMAVAR,* J. I. BUDNICK,* H. C. HAYDEN,* P. A. [illegible],** AND V. PATARINI**
*The University of Connecticut, Storrs, CT 06268,
**United Technologies Research Center, East Hartford, CT 06108

ABSTRACT

The dependence of the implanted layer composition on total dose, dose rate and target chamber environment for Cr^+ implanted Si have been studied by means of Rutherford Back Scattering (RBS) and Auger Electron Spectroscopy (AES). Implantation of Cr^+ for doses up to 2×10^{17} ions/cm^2 and a fixed dose rate and energy were carried out in an ultra high vacuum (UHV) system as well as in a diffusion pumped vacuum (DPV) system. For the former, the maximum Cr concentration was about 42%. On the other hand, implantation of Cr in a DPV system resulted in a much higher peak concentration (86%) and retention.

Both the RBS and AES results positively demonstrate the existence of extensive surface carbon for a Si-rich surface and a chromium oxide layer for the Cr-rich surface. This result suggests that the interaction of oxygen or carbon occurs preferentially and depends on the surface composition.

No surface compositional variation could be observed by the RBS experiments for Cr implanted in a UHV system for different dose rates. In contrast, for implantation in a DPV system, higher concentrations can be achieved for lower dose rates.

INTRODUCTION

In this work we are interested in: (i) investigating silicide formation by means of the high dose implantation technique for the Cr-Si system, (ii) obtaining information concerning the saturation concentration of implanted Cr into Si in an ultra high vacuum as well as in a DPV system, and (iii) determining the nature of the final products for different vacuum conditions as well as understanding the effect of oxygen and carbon impurities on compound formation or precipitation.

The maximum achievable concentration in ion implanted systems is governed by the sputtering of the near surface region of the target system [1]. Implantation in a vacuum system with a pressure in the order of 10^{-6} Torr may, in some cases, result in the production of an oxide or carbide layer where generally such a layer can reduce the sputtering rate. Armenian et al. [2] reported the production of a very high concentration of Cu for Cu implantation in Al as a result of the creation of an oxide layer on their target.

Introduction of elements of residual adsorbed gases by recoil implantation [3] or any other means [4] has two factors: (1) a detrimental effect, i.e., the target becomes contaminated with unwanted impurities; and

Mat. Res. Soc. Symp. Proc. [illegible] (1984) © Elsevier [illegible]

of the stress relief effect reported here; thus, other bombardment energies could be investigated. With the present state of experimental results, the generality of the effect is not established; however, there is evidence that, whatever the nature of the deformation produced by atomic peening, this deformation may be largely removed by bombardment with very high energy ions that reach and intermix the interfacial region of the sample.

ACKNOWLEDGMENTS

The authors wish to express their appreciation to Quentin Kessel and John Giannopolis for use of the University of Connecticut Van de Graaff facility. Also, thanks are in order to Cliff Schuman for invaluable assistance with the X-ray apparatus and to Eva Wood for assistance with the microprobe analysis.

The work at the University of Connecticut was supported in part by the Office of Naval Research and the work at the University of Leuven was supported by the Belgian Interuniversitair Institut voor Kernwetenschappen.

REFERENCES

1 F. d'Heurle, *Metall. Trans.*, *1* (1970) 725.
2 A. G. Blachman, *Metall. Trans.*, *2* (1971) 699.
3 J. A. Thornton and D. W. Hoffman, *J. Vac. Sci. Technol.*, *14* (1977) 164.
4 D. W. Hoffman and J. A. Thornton, *Thin Solid Films*, *50* (1977) 355.
5 J. J. Cuomo, J. M. E. Harper, C. R. Guarnieri, D. S. Yee, L. J. Attanasio, J. Angilello and C. T. Wu, *J. Vac. Sci. Technol.*, *20* (1982) 349.
6 P. V. Plunkett, R. M. Johnson and C. D. Wiseman, *Thin Solid Films*, *64* (1979) 121.
7 D. W. Hoffman and J. A. Thornton, *Thin Solid Films*, *45* (1977) 387.
8 D. W. Hoffman and M. R. Gaerttner, *J. Vac. Sci. Technol.*, *17* (1980) 425.
9 C. C. Koch, J. O. Scarbrough and D. M. Kroeger, *Phys. Rev. B*, *9* (1974) 888.
10 M. H. Read and D. H. Hensler, *Thin Solid Films*, *10* (1972) 123.
11 J. S. Kasper and K. Lonsdale (eds.), *International Tables for X-ray Crystallography*, Vol. II, Kynoch, Birmingham, 1967, p. 167.
12 Namavar *et al.*, to be submitted.
13 E. Witt and R. W. Vook, *J. Appl. Phys.*, *39* (1968) 2773.
14 B. D. Cullity, *Elements of X-Ray Diffraction*, Addison-Wesley, Reading, MA, 1956.
15 W. B. Pearson, *A Handbook of Lattice Spacings and Structures of Metals and Alloys*, Pergamon, New York, 1958, p. 769.

niobium. Witt and Vook have calculated theoretical strain ratios $\varepsilon_\perp/\varepsilon$ for a number of cubic films of various orientations, where $\varepsilon_\perp$ is the strain perpendicular to the surface and ε is the strain in any direction parallel to the film surface[13]. The theory of Witt and Vook is valid for the case in which all stresses acting on the film are applied at the interface between the film and the substrate. Without a better knowledge than now exists with regard to the mechanism by which sputtered films tend to be compressively stressed, it is not clear to what extent the assumption of interfacial stresses is valid in the present case. Despite this caveat, it may be of some interest to compare the present results on the as-deposited film with predictions based on the Witt and Vook calculation. For the [110] orientation of niobium, $\varepsilon_\perp/\varepsilon$ is calculated by Witt and Vook to have a value of -1.306. If we refer to Fig. 1, it is evident that an expansion of the niobium lattice such as to increase the distance between (101) planes will result in a monoclinic distortion of the unit cell. Using the above theoretical value of $\varepsilon_\perp/\varepsilon$, assuming d_{101} to correspond to the diffractometer result and assuming the unstressed film to be pure niobium, we may deduce the corresponding values of b and c, as well as angle β in Fig. 1(b). (Clearly, $a = c$ in the monoclinically distorted cell.) The relation between the interplanar distance d_{hkl} and the values of a, b and β for such a monoclinic cell is given by the expression

$$\frac{1}{d_{hkl}^2} = \frac{1}{\sin^2\beta}\left(\frac{h^2}{a^2} - \frac{2hl\cos\beta}{a^2} + \frac{l^2}{a^2} + \frac{k^2\sin^2\beta}{b^2}\right) \tag{1}$$

where h, k and l are Miller indices[14]. Using the above expression, we may determine a value of d_{310} and therefore a_{310} where, *in the present case*, a_{310} is *defined* in terms of the expression for a cubic cell as follows:

$$a_{hkl} = d_{hkl}(h^2 + k^2 + l^2)^{1/2} \tag{2}$$

If the above procedure is carried out and the lattice constant of pure unstressed niobium when rounded off to an accuracy of three decimal places is assumed to be given by $a = 3.301$ Å [15], the "predicted" value of a_{310}, as defined by eqn. (2), is also 3.301 Å. This value is near the lower limit of the error bar for the a_{310} value of as-deposited niobium as shown in Fig. 5. There is therefore an indication of some degree of expansion of the unit cell volume for the as-deposited niobium relative to the case in which absolutely pure niobium was stressed at the interface alone.

4. DISCUSSION

Sputtered metal films are often found to be under compressive stress, and work by other investigators indicates that this stress may be due to some structural deformation associated with mechanical bombardment by the sputtering gas. On the basis of the present work alone, it would have been tempting to speculate that this deformation arises, in part, from a registration mismatch at the interface with the substrate which is "unlocked" by ions sufficiently energetic to reach and intermix the interface region. However, the fact that the compressive stress phenomenon is observed for many different types of substrates such as glass wafers[8], Si_3N_4-coated silicon wafers[5] and oxidized silicon[1] is strong evidence against a lattice mismatch effect.

It would be of interest to extend the present study to investigate the systematics

radiation. Measurements of the (310) reflection were made using a 10° glancing angle, Co Kα radiation and a Bragg angle of 58.5°, and also using a 20° glancing angle, Fe Kα radiation and a Bragg angle of 67°. Since the (310) and (202) planes have an interplanar angle close to 48°, the above conditions placed the (310) reflection on the film axis.

The quantities a_{310} and a_{202} are now defined as those values of the lattice constant which would result if one applied the usual relation between lattice constant and interplanar separation for a cubic material to the measured values of the interplanar distances d_{310} and d_{202}. There was no detectable difference, to within an error bar determined by the halfwidth of the film lines, between the niobium a_{310} values obtained using a cobalt source and a 58.5° Bragg angle and those obtained using an iron source and a 67° Bragg angle. This last result indicates that systematic errors in the experimental lattice constant were not important for the region of Bragg angle near that of the niobium (310) reflection. Additional evidence for the accuracy of these Read camera lattice constants was obtained by comparing Read camera and diffractometer results for the interplanar distances of the (202) surface-parallel planes. By orienting the sample at 56° incident angle and observing the (202) reflection with a Read camera and Fe Kα radiation, it was found that Read camera values for d_{202} agreed with diffractometer values. Since good agreement with a well-aligned diffractometer was thereby attained using a reflection at a Bragg angle of 56°, it was inferred that the (310) reflection, which can be measured at a still larger Bragg angle (67°), can also be measured with sufficient accuracy for the present purposes.

Figure 5 shows a plot of a_{202} *versus* a_{310} for the as-deposited, the 300 keV bombarded and the 600 keV bombarded samples. a_{310} was determined using a 20° glancing angle and Fe Kα radiation, as described above. Figure 5 shows that the as-deposited sample is distorted from a cubic cell. The 300 keV sample maintains this distortion but with an expanded cell volume. The 600 keV sample has a nearly cubic cell but with a slightly expanded lattice constant relative to that of pure bulk

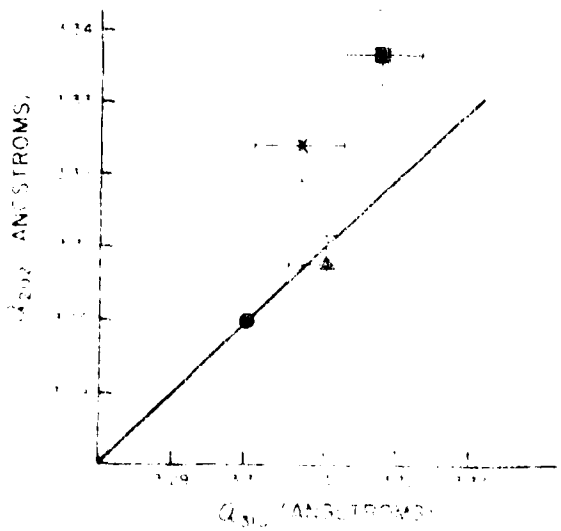

FIG. 5—a_{202} vs a_{310} for [illegible] samples. ——, locus of points corresponding to an undistorted cubic cell; ▲, 600 keV bombarded sample; ■, 300 keV bombarded sample; ×, as-deposited sample; ●, ideal niobium lattice constant. The quantity a_{202} is defined as that lattice constant that would result for a cubic cell with d_{202} as determined [illegible] even though the actual cell may have a monoclinic distortion.

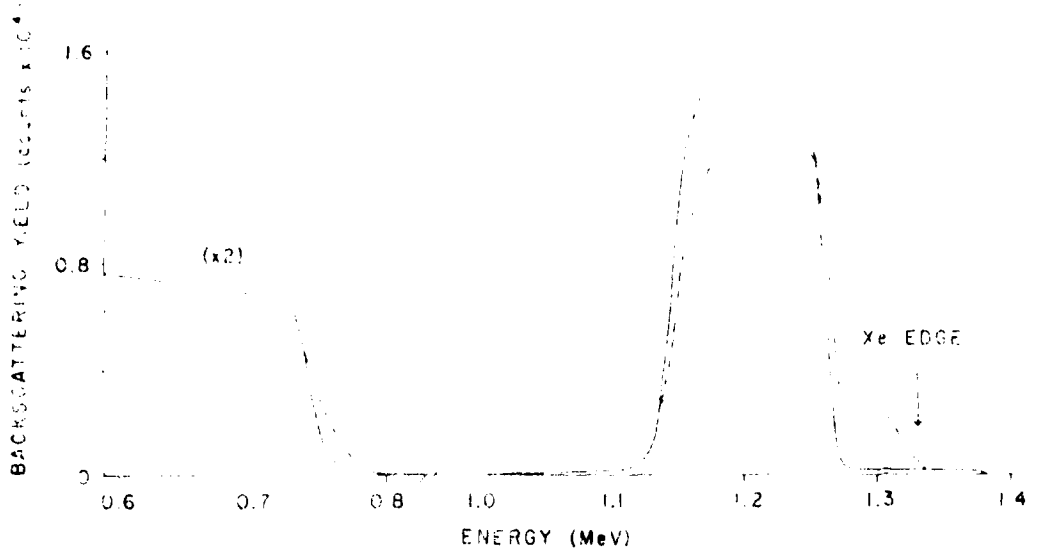

Fig. 3. Rutherford backscattering spectrum (1.5 MeV $^4He^+$) of a sample (1000 Å niobium on Si (111)) implanted with 300 keV xenon (——) compared with an unimplanted specimen (- - -). Energies below 0.8 MeV correspond to backscattering from silicon.

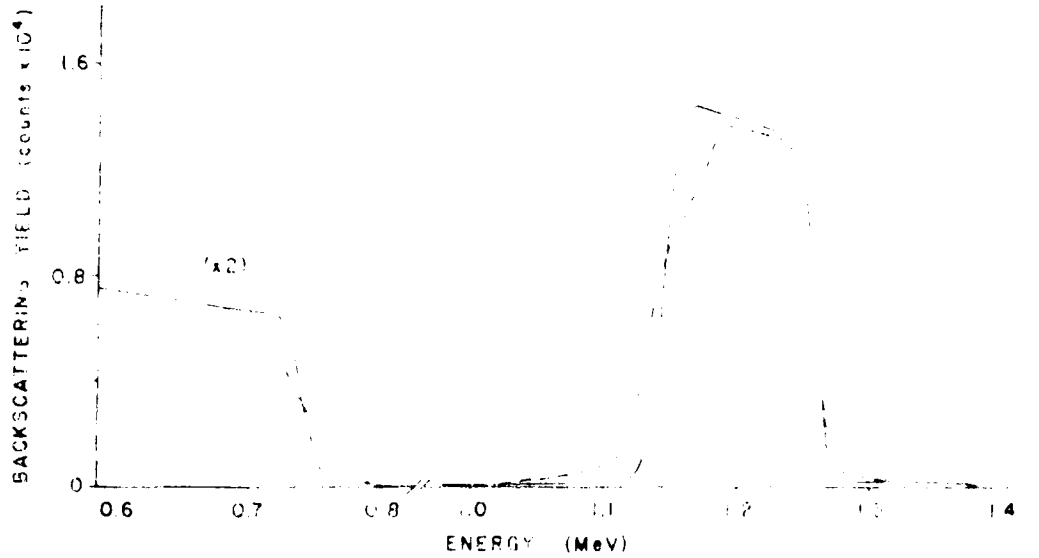

Fig. 4. Rutherford backscattering spectrum (1.5 MeV $^4He^+$) of a sample (1000 Å niobium on Si (111)) implanted with 600 keV xenon (——) compared with an unimplanted specimen (- - -). Energies below 0.8 MeV correspond to backscattering from silicon.

of these Rutherford backscattering spectra, to be discussed elsewhere[14], is outside the range of discussion of the present paper.

To return to the discussion of the X-ray results, it should be pointed out that the diffractometer results furnish information about the interplanar distance only for planes parallel to the sample surface. It was desirable to obtain lattice spacing information from other sets of planes as well by means of a Read camera. Although a Read camera is not designed to be particularly suited for precision lattice constant measurements, the accuracy of the results was shown to be sufficient for present purposes, provided only that the niobium reflections furthest into the back reflection region were used. The largest and therefore most accurate Bragg angle obtainable for niobium was that corresponding to the (310) reflection and Fe Kα

Fig. 5: RBS spectra of Al implanted into Si (111) and Si (100) (UHV).

and a dose rate of 2.4 x 10^{14} ions/cm^2 and doses ranging from 3 to 10 x 10^{17} ions/cm^2 resulted in Al segregation where Al is preferentially oriented in a (111) plane parallel to the (111) plane of the Si substrate. On the basis of RBS Fig. 1, AES Fig. 2 and x-ray results, we may conclude that for implantation of Al with a dose of 3 x 10^{17} ions/cm^2 Al islands are formed where they occupy about 30% of the surface sample. However, as the supply of Al increases by increasing the dose of implantation to 1 x 10^{18} ions/cm^2, the surface density of these islands increases and eventually an Al-rich layer with a thickness of approximately 2500Å is created. It is expected that the near surface region of Si targets becomes highly disordered (amorphized) because of high dose implantation. However, it is intriguing that Al precipitates possess a preferred (111) orientation.

Very recently Kaufmann et al. [8] reported that as a result of implantation at room temperature of silver into a single crystal of beryllium, silver precipitates at room temperature such that the (111) axis in silver is parallel to the (0001) axis of the beryllium target. Furthermore, Tsaur et al. [9] reported the formation of (111) preferred orientation in ion beam mixed Au-Ni, Ag-Cu and Au-Co systems.

On the other hand, our x-ray diffraction measurements, of implanted Al into Si (111) in an ultra clean vacuum system, suggests that, although Al segregates, it possesses a polycrystalline structure. Since implantation conditions for samples prepared in UHV and UHPV systems were the same except for the pressure, we believe that the formation of highly oriented Al films is probably related to impurities, possibly oxygen and carbon, which were introduced during implantation in the UHPV system. At high doses, for implantation in a clean system, Al is present at a greater depth than that expected from the projected range calculation (Fig. 5). For poor vacuum conditions, though, the segregated Al remains at the near surface region.

Results shown in Figs. 4 and 5 suggest that for the implantation of Al

in Si in an ultra clean or moderately clean vacuum system, implanted Al redistributes during implantation or during post-implantation room temperature annealing. Implanted atoms have a tendency to penetrate deeper as the dose of implantation increases (see Fig. 4). There is a similarity between the results of this work and those reported by Rusbridge [4] for implanted Al into AlGe at 160°C.

At the present time, interpretation on the redistribution of Al in our work in comparison to the interpretation of AlGe results [10] is hindered because of the lack of detailed information on depth profiles for implanted Al in Si.

No Al segregation was observed for Al implanted Si (UDPV) with a low dose rate and for doses of up to 5×10^{17} ions/cm^2. In contrast, implantation under similar conditions, even in an oil trapped DPV system resulted in Al segregation. From these results, it seems that during high dose rate implantation in the UDPV system, fewer contaminated elements were available because of the sputtering effects and the short times required for implantation. Secondly, precipitated nucleation for implanted Al occurred as soon as the Al concentration at the damage peak surpassed the solubility limit and before any contaminant has a chance to diffuse to the damage peak. On the other hand, for low dose rate implantation in UDPV systems, contaminant atoms such as carbon may reach damage peaks faster than implanted Al reached its solubility limit. Probably the presence of very chemically active small impurities such as carbon and oxygen could act as a sink for defects which as a result delay or prohibit Al precipitation.

#Supported by the Office of Naval Research.

REFERENCES

1. F. Namavar, J.I. Budnick and F.A. Otter, Thin Solid Films 104 (1983) p. 31.
2. F. Namavar, J.I. Budnick and F.A. Otter, unpublished data, 1983.
3. S.S. Lau, B.Y. Tsaur, M. von Allmen, J.W. Mayer, B. Stritzker, C.W. White and B. Appleton, Nuclear Instruments and Methods 182/183 (1981) pp. 97-105.
4. K.L. Rusbridge, Nuclear Instruments and Methods 182/183 (1981) p. 521.
5. K.L. Bertram, F.J. Minter, J.A. Hudson and K.C. Russell, Journal of Nuclear Materials 75 (1978) p. 42.
6. M.R. Mruzik and K.C. Russell, Journal of Nuclear Materials 78 (1978) p. 343.
7. H. Jones and C. Suryanarayana, Journal of Materials Science 8 (1973) p. 705.
8. E.N. Kaufmann and L. Buene, Nuclear Instruments and Methods 182/183 (1981) p. 327.
9. B.Y. Tsaur, S.S. Lau, L.S. Hung and J.W. Mayer, Nuclear Instruments and Methods 182/183 (1981) p. 67.
10. A.P. Marwick in Surface Modification and Alloying, edited by J.M. Poate, G. Foti and D.C. Jacobson (Plenum Press, New York and London, 1983), p. 211.

ACKNOWLEDGMENTS

We are very grateful to Professor Quentin Kessel for his help with the Van de Graaff accelerator, to Professor D. I. Potter for allowing us to use his ultra high vacuum implantation chamber and to M. Ahmed for his assistance during implantation. In addition, we would like to thank R. Roser, P. Clapis, John Gianopoulous and C. H. Koch for their technical assistance.

Nuclear Instruments and Methods in Physics Research B8 (1985) 357–360
North-Holland, Amsterdam

NUCLEAR RESONANCE PROFILING OF HIGH DOSE IMPLANTS OF Al IN Si *

F. NAMAVAR, J.L. BUDNICK and E.H. SANCHEZ **
The University of Connecticut, Storrs, CT 06268, USA

F.A. OTTER
United Technologies Research Center, East Hartford, CT 06108, USA

We have applied nuclear resonance profiling (NRP) techniques to determine the depth distribution of implanted Al into Si. For implantation of Al at 200 keV and at doses of up to 10^{18} Al/cm^2, our results indicate that the depth distribution of Al implanted in an ultra-high vacuum (UHV) system ($\simeq 10^{-8}$ Torr) is independent of dose rate and target orientation. For a dose of 10^{18} Al/cm^2 a single Al distribution was observed with an Al concentration of about 65% at peak while 85% of the implanted Al was retained in the Si target.

On the other hand, the depth distribution of implanted Al in a diffusion pumped vacuum (DPV) system ($\simeq 10^{-6}$ Torr) was greatly influenced by dose rates and target orientation. For high dose rate implantation (40–50 μA/cm^2) the depth distribution of Al appeared to be bimodal or broadened and about 95% of the implanted Al is retained in the Si target. A peak Al concentration of up to 75% could be obtained.

1. Introduction

It has been known for some time [1,2] that implantation in a poor vacuum system ($\simeq 10^{-6}$ Torr) results, in some cases, in the formation of a surface oxide or a carbon layer. A surface oxide or carbon layer may reduce surface sputtering, thus making it possible to achieve a higher concentration of implanted atoms. The effects and significance of a contaminant surface layer formed during implantation on the implantation processes have been recognized [2,3]. However, the number of reported papers which deal with the problem is very limited [3]. Furthermore, to date, no detailed studies have been reported for high dose implantation of metals into a Si system.

Recently, we initiated a study to understand the effect of vacuum conditions on the composition and structure of implanted layers for high dose implantation of Al and Cr into Si [4,5]. Samples were prepared by implanting both metals in UHV($\simeq 10^{-8}$ Torr) and DPV ($\simeq 10^{-6}$ Torr) systems into Si (111) and Si (100) with doses of up to 10^{18} ions/cm^2.

We have applied RBS, AES and X ray analysis techniques to these studies. For the Al implanted samples, except those prepared in a DPV system ($\simeq 10^{-6}$ Torr) at a low dose rate (5 μA/cm^2), X-ray analysis indicates Al segregation. For the implantation of Al in a DPV system, the structure of segregated Al is generally influenced by dose rate and target orientation in contrast to implantation in a UHV system ($\simeq 10^{-8}$ Torr) in which the structure of segregated Al is independent of target orientation as well as dose rate. For samples prepared in a DPV system ($\simeq 10^{-6}$ Torr) with a high dose rate implantation in Si (100), segregated Al possesses a polycrystalline structure while for Si (111), segregated Al possesses a (111) preferred orientation. RBS indicates the presence of an appreciable surface

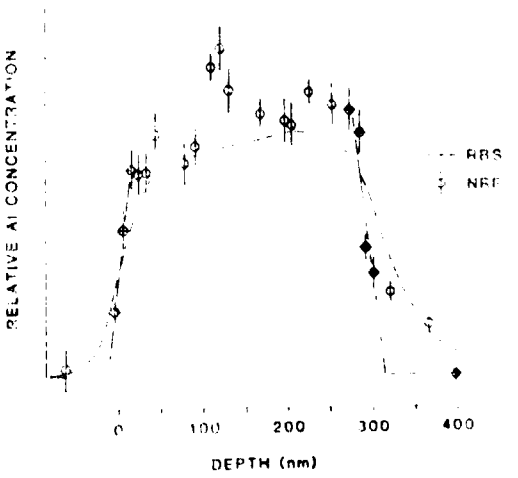

Fig. 1. NRP data and RBS spectrum for deposited [illegible] energy [illegible] are compared.

* Supported in part by the Office of Naval Research and also by The University of Connecticut Research Foundation.
** On a fellowship from CONICET, Argentina.

0168-583X/85/$03.30 © Elsevier Science Publishers B.V.
(North-Holland Physics Publishing Division)

carbon layer only for those samples implanted at a low dose rate ($\simeq 5\ \mu A/cm^2$) in a DPV system. For samples implanted with a high dose rate ($\simeq 40\ \mu A/cm^2$) in a DPV system, RBS does not indicate the presence of any carbon or oxygen. However, AES suggests the presence of distributed carbon and oxygen [4].

Because the backscattered signals for Al into Si are superimposed on each other, a precise knowledge about the depth profile of Al in Si cannot be obtained by RBS experiments. Therefore, we have applied nuclear resonance profiling (NRP) using the $^{27}Al\ (p, \gamma)^{28}Si$ reaction in order to determine the depth profile of implanted Al into Si.

2. Experimental procedures

Polished single crystals of Si with (111) and (100) orientations were uniformly implanted with 100 keV Al^+ ions by means of the high current implanter of The University of Connecticut. During implantation three parameters were varied:

1) dose, ranging from 1×10^{17} to 1×10^{18} ions/cm^2;
2) dose rate, ranging from 3×10^{13} to 3×10^{14} ions/cm^2 s;
3) vacuum conditions, diffusion pumped vacuum system $(2\text{-}4) \times 10^{-6}$ Torr and an ultra-high vacuum (UHV) system $(2\text{-}4) \times 10^{-8}$ Torr.

During implantation, RBS and NRP samples were fastened to the heat sink with conducting materials (silver paint). The temperature of the high dose rate implanted samples was monitored with the help of thermocouples and an infrared pyrometer which was sensitive to temperatures above 50°C. No measurable rise in target temperature could be observed.

Implantation and RBS were carried out while samples were tilted to 10° from the normal incidence of the ion beam. On the other hand, for NRP experiments, samples were tilted to 30° and 60° with respect to the proton beam. 1.78 MeV γ rays, produced in a 992 keV narrow resonance line in the $^{27}Al(p, \gamma)^{28}Si$ reaction, were observed by a 7.5 cm thick NaI(Tl) scintillator detector that was placed perpendicular to the beam. In each run an Al target was used to monitor the accelerator calibration as well as to obtain the ratio of γ-radiation from Al implanted samples to bulk Al. In the course of the NRP experiments, different regions of the same sample were studied in order to minimize the effect of ion beam mixing, sputtering and possible carbon build-up on sample surface.

He^+ and H^- beams were provided by means of 2 MeV Van de Graaff accelerator of The University of Connecticut. The energy resolution of the accelerator was about 0.5 keV and was defined by beam aperture and the deflecting angle of the proton beam, after passing through the analyzing magnet.

In fig. 1, we have compared a 1.5 MeV He^+ backscattering spectrum with NRP data for deposited 3000 Å Al on grafoil (C). NRP data presented here is the average value of 2 to 3 independent runs. RBS spectrum of deposited Al on grafoil (not shown) positively identified the large amount of oxygen on the Al surface and the Al/C interface (4 and 3×10^{16} O/cm^2, respectively). We believe that the presence of aluminum oxides at the surface and interface partially influenced our NRP results. However, from fig. 1 it is clear that much better depth resolution and accuracy can be achieved with NRP experiments as compared with standard RBS experiments for a 3000 Å Al on grafoil (C).

3. Experimental results

3.1. Implantation in a UHV system ($\simeq 10^{-8}$ Torr)

Fig. 2 demonstrates the results of the NRP experiments for implanted Al with 100 keV into Si (111) and Si (100) in a UHV system to a dose of 1×10^{18} Al/cm^2 with low (10 μA/cm^2) and high (50 μA/cm^2) current density implantation. These results clearly indicate that Al distribution for implantation in a UHV system is independent of dose rate or target orientation. Furthermore, it is also proof of the reproducibility of our detection system and implantation. Fig. 2 suggests that for a dose of 1×10^{18} Al/cm^2 a concentration of 6% could be achived, while 85% of implanted Al was retained in the Si target. (X-ray diffractometer analysis of all of these samples indicates the presence of metallic polycrystalline Al.)

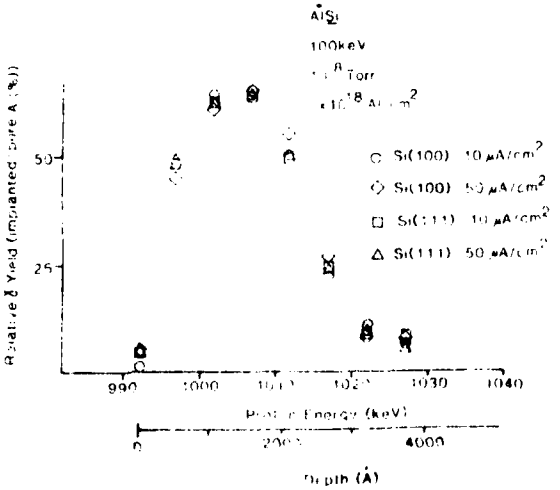

Fig. 2. NRP results for low and high dose rate implantation into Si (111) and Si (100) in a UHV system ($\simeq 10^{-8}$ Torr). These results clearly demonstrate the reproducibility of our implantation and detection systems.

The average values obtained from moment calculations [6] of experimental data (fig. 2) for Al distribution are as follows: $\mu = 1570$ Å (mean), $\sigma = 812$ Å (straggling), $\beta_1 = 0.25$ (skewness) and $\beta_2 = 2.86$ (kurtosis). The experimental values obtained for the mean and straggling are in good agreement with the theoretical calculation [7]. Furthermore, β_1 and β_2 values suggest that the depth distribution of Al only slightly deviated from a normal distribution where $\beta_1 = 0$ and $\beta_2 = 3$.

3.2 *Implantation in a DPV system ($\simeq 10^{-6}$ Torr)*

We have measured the depth distribution of implanted Al with 100 keV into Si (111) and Si (100) with a low dose rate ($\simeq 5\ \mu A/cm^2$) and high dose rate ($\simeq 50\ \mu A/cm^2$) in a DPV system (10^{-6} Torr) by the NRP technique. Our results clearly indicate that depth distribution of implanted Al is greatly influenced by dose rate and target orientation and disagrees with results obtained for those samples for which implantation was carried out in a UHV system. For high dose rate ($\simeq 50\ \mu A/cm^2$) implantation, the depth distribution of implanted Al generally appeared to be bimodal or considerably broadened. For low dose rate ($\simeq 5\ \mu A/cm^2$) implantation, however, the Al depth profile emerges at the greater depth because of the large amount of carbon agglomeration on the Si surface (see fig. 3 of ref. [4]).

Fig. 3 compares the NRP results for samples implanted with a dose of 1×10^{18} Al/cm^2 and a dose rate of 40–50 $\mu A/cm^2$ into a Si (111) target in a UHV system ($\simeq 10^{-8}$ Torr) and a DPV system ($\simeq 10^{-6}$ Torr). NRP results for implantation in a DPV system indicate that Al distribution is broadened; a large Al distribution appears in the near surface region along with a component of Al distribution which extends to a greater depth.

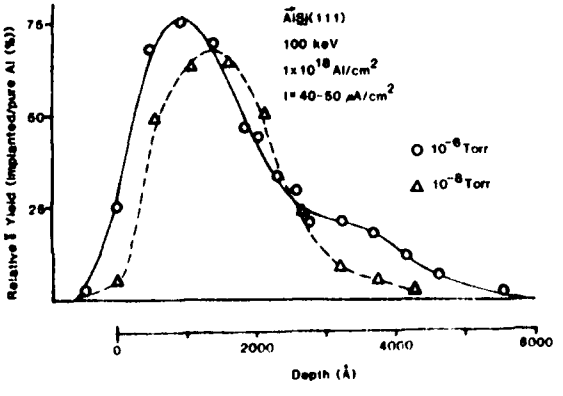

Fig. 3. NRP results compared for implantation of Al under similar conditions except for vacuum condition. Higher Al concentration and retention is another feature to bimodal distribution for implantation in a DPV system ($\simeq 10^{-6}$ Torr).

4. Discussion and conclusion

The dependency of the depth distribution of room temperature implantation in Si on vacuum conditions has been demonstrated by means of nuclear resonance profiling. The results obtained for samples implanted in a UHV system ($\simeq 10^{-8}$ Torr) show that the depth distribution of implanted Al is independent of dose rate and target orientation in contrast to implantation in a DPV system in which Al distribution is influenced by dose rate and target orientation. The high concentration (65%) and retention (85%) for Al implanted in a UHV system with a dose of 1×10^{18} Al/cm^2 suggests that very few atoms from the target systems are sputtered during implantation. Indeed, from the recent theoretical work of Matsunami et al. [8], one can easily derive the sputtering yield for the implantation of Al with 100 keV into Si to be about 0.75. For a sputtering yield of less than one, an increase in the number of atoms in the implanted region is expected simply because more atoms are introduced on the near surface layer than leave the target surface. Therefore, one should assume that sample swelling or change in density should occur. The latter, combined with the NRP results, may clarify the misunderstood RBS spectra for the Al implanted sample (see fig. 5 of ref. [4]). NRP results (fig. 2) suggest that the mean penetration for Al is about 1570 Å which is quite in agreement with the theoretical value [7].

Furthermore, considering the experimental value obtained (fig. 2) for the mean, straggling, skewness and kurtosis suggests that the depth distribution of Al as obtained by NRP experiment is only slightly different from a normal distribution. Further, RBS spectra indicate (fig. 5 of ref. [4]) about 70% of target surface is Si. Therefore, we conclude with a dose of 1×10^{18} Al/cm^2 and 100 keV energy, one cannot reach a steady state concentration for Al.

High dose rate implantation in Si (111) [in a DPV system (10^{-6} Torr)] resulted in Al redistribution where a large portion of Al moves to the sample surface and a smaller portion penetrates to a greater depth. Such a behavior was not observed for low dose rate implantation into Si (111) or high dose rate implantation into Si (100).

First of all, we should emphasize that the above results are real and are not artifacts of NRP or due to energy straggling at a depth of a few thousand Å, because RBS and AES data (figs. 1 and 2 of ref. [4]) are in agreement with NRP results and because we have demonstrated the ability of NRP in fig. 1 for 3000 Å Al on C. We have shown that for our measurement the effect of energy straggling is less important in compari

son to a standard RBS. Moreover, the Al shift toward the surface could by no means be due to straggling and shift at greater depth is more than 1000 Å.

Secondly, the nature of this redistribution is not due to sputtering because in a DPV system ($\simeq 10^{-6}$ Torr), oxygen and carbon are incorporated in the target surface and sputtering rate from surface is further reduced. Indeed, higher Al concentrations ($\simeq 75\%$) and retention (95%) have been observed for implantation in a DVP system compared with implantation in a UHV system.

Such a distribution cannot be due to the channeling effect during Al implantation because similar behavior was not observed for samples prepared in a UHV system with identical implantation conditions (except for vacuum pressure). Moreover, it is expected that implantation with a dose of about 10^{15} ions/cm^2 totally amorphizes the implanted region.

On the other hand, the only condition which these two groups of samples do not share is the presence of oxygen and carbon in the implanted region. Incorporated impurities may have influenced depth distribution by two means: (1) facilitated Al or Si migration and (2) creating a larger stress field due to higher Al and impurity concentrations.

We are very grateful to Prof. Quentin Kessel and Prof. Howard Hayden for their help with the Van de Graaff accelerator and implantor, to Prof. D.I. Potter for allowing us to use his UHV implantation chamber, and to Dr. Roger Kelly for providing us with literature on sputtering. In addition, we would like to thank R. Roser, P. Clapis, J. Gianopoulous and C.H. Koch for their technical assistance.

References

[1] F. Arminen, A. Fontell and V.K. Lindross, Phys. Stat. Sol. (a) 4 (1971) 663.

[2] Z.L. Liau and J.W. Mayer, J. Vac. Sci. Technol. 15(5) (1978) 1.

[3] Z.L. Liau and J.W. Mayer, in: Surface Modification and Alloying, eds., J.M. Poate, G. Foti and D.C. Jacobson (Plenum, New York and London, 1983) p. 10.

[4] F. Namavar, J.I. Budnick, A. Fasihuddin, H.C. Hayden, P.A. Pease, F.A. Otter and V. Patarini, Mat. Res. Soc. Symp. Proc. 27 (1984) 347.

[5] F. Namavar, J.I. Budnick, H.C. Hayden, F.A. Otter and V. Patarini, Mat. Res. Soc. Symp. Proc. 27 (1984) 341.

[6] M. Kendall and A. Stuart, The Advance Theory of Statistics, vol. 1 (Hafner., New York, 1969).

[7] A.F. Burenkov, F.F. Komarov, M.A. Kumahov and M.M. Temkin, Tables of Parameters for Spatial Distribution of Implanted Ions (State University of White Russia, Minsk, USSR, 1980) in Russian.

[8] N. Matsunami, Y. Yamamura, Y. Itikawa, N. Itoh, Y. Kazumta, S. Miyagawa, K. Morita, R. Shimizu and H. Tawar, Internal Report, Nagoya University, Nagoya, Japan (1983).

CHEMICAL PROFILING AND STRUCTURAL STUDIES OF ION-BEAM-MIXED ALUMINUM ON SILICON*

Thin Solid Films, 104 (1983) 31–41

F. NAMAVAR AND J. I. BUDNICK
Department of Physics, University of Connecticut, U-46, Storrs, CT 06268 (U.S.A.
F. A. OTTER
United Technologies Research Center, East Hartford, CT 06108 (U.S.A.)
(Received December 14, 1982; accepted December 20, 1982)

The ion beam mixing technique has been applied to the production of Al–Si thin alloy layers as an alternative method to thermal annealing. Both unimplanted deposited aluminum thin films on silicon substrates and films implanted with energetic xenon ions were studied by Rutherford backscattering, channeling, secondary ion mass spectroscopy, nuclear resonance profiling and scanning electron microscopy techniques. The results of these experiments indicate that (i) intermixing between aluminum and silicon became observable when the implantation dose of energetic xenon through the interface surpassed 2×10^{16} ions cm^{-2}; (ii) intermixing is dependent on the dose but not on the dose rate of implantation; (iii) damage to the silicon substrate extended only to the region penetrated by implanted ions; (iv) the Al–Si alloy layer region is uniform in texture and no segregation can be observed. Moreover, the integrity of the alloy layer is retained for a long period of room temperature annealing.

1. INTRODUCTION

Thermal reactions between deposited aluminum thin films on silicon substrates have been extensively studied because of their technical importance[1,2]. During thermal annealing at temperatures below the Al–Si eutectic (577 C), silicon migrates and dissolves into the aluminum overlayer[3]. However, the dissolution of the Al–Si interface occurs non-uniformly and forms pits[4,5]. Moreover, because the solubility of silicon decreases with decreasing temperatures, aluminum becomes supersaturated during the cooling process and precipitation[6,7] and epitaxial growth[8,9] may occur. The latter problem has also been observed for codeposited silicon and aluminum[1] as well as for silicon post-evaporated onto the aluminum layer[10].

During the past few years[11,12], the capability of the ion beam mixing technique to intermix deposited metal films with silicon substrates has been demonstrated. However, no reported attempt has been made to explore the possibility of forming a

* Paper presented at the Symposium on Interfaces and Contacts, Boston, MA, U.S.A., November 2–4, 1982.

0040-6090/83/$3.00

uniform Al–Si alloy layer by the new technique. Al–Si and Au–Si both exhibit a simple eutectic behavior. It has been shown, though, that the ion-induced amorphous Au–Si layer is unstable even on room temperature annealing and decomposes to an equilibrium mixture of gold and silicon via the metastable crystalline phase[13]. From the onset of this work we believed that the integrity of the xenon-ion-induced alloy layer might be preserved (at least for room temperature annealing) because (i) the eutectic temperature (577 °C) of the Al–Si system is much higher than the eutectic temperature (370 °C) of the Au–Si system and (ii) implanted oversize impurities in nickel such as xenon, tellurium and silver trap vacancies[14]. Similar results were observed and have been reported for other host materials (see for example ref. 15). If xenon atoms present in the surface region act as vacancy trappers, the migration of aluminum and silicon which results in segregation would therefore be retarded.

The ion beam mixing of aluminum thin film on silicon substrates as well as the lateral uniformity and stability of the intermixed alloy layer is the subject of this work. The Rutherford backscattering (RBS) technique was the major analyzing tool used to observe the effect of xenon implantation in the Al/Si system. However, because signals from aluminum and silicon overlap, the precise determination of the aluminum-to-silicon ratio in the intermixed region becomes difficult. Therefore we have studied some of the samples by secondary ion mass spectroscopy (SIMS) as well as by nuclear resonance profiling (NRP) using the $^{27}Al(p,\gamma)^{28}Si$ reaction.

Special attention has been given to the stability of the ion-induced Al–Si alloy layer. As we shall demonstrate, the integrity of the ion-induced Al–Si alloy was retained for a long period of room temperature annealing.

2. EXPERIMENTAL PROCEDURES

Aluminum films with thicknesses ranging from 300 to 1000 Å were deposited simultaneously onto ⟨111⟩-oriented silicon disks with a 2.5 cm diameter as well as onto carbon substrates by electron beam evaporation from a crucible made of graphite. The substrates were located about 10 cm from the crucible. The vacuum system was a diffusion-pumped system with a liquid nitrogen trap. Starting pressures were typically 10^{-7} Torr, and pressures rose to about 10^{-5} Torr during evaporation.

Sample surfaces were tilted to 5° from the normal incidence of the ion beam both for RBS experiments and for implantations. RBS data were analyzed by measuring the energy spectra of He^+ ions with an initial energy of 1.5 MeV backscattered to an angle of 170°. RBS experiments were carried out for each individual Al/Si and its associate Al/C sample in order to measure the thickness of aluminum thin films and to determine whether impurities were present. The results of RBS on Al/C indicate only the presence of a small amount of oxygen both at the interface and on the aluminum surface. However, the total amount of oxygen present at the interfaces or on the surfaces was less than 2×10^{16} atoms cm^{-2}.

Energetic Xe^+ ions were used in order to initiate intermixing of aluminum and silicon. During the experiment, samples were fastened to the heat sink (sample holder) with silver paint. The energy of the Xe^+ ions was varied (150–300 keV) and was in proportion to each particular aluminum film thickness. Samples were

implanted uniformly in an area of 0.4 cm^2 while the area studied by RBS was confined to 1 mm^2. RBS spectra of virgin and xenon-implanted Al/Si samples were recorded just as implantation was terminated (without exposing the samples to air). RBS spectra were also recorded after annealing of samples at room temperature for several weeks. Dose and dose rate dependences of intermixing were studied with doses ranging from 5×10^{15} to 1.1×10^{17} ions cm^{-2} and dose rates ranging from 10^{12} to 10^{13} ions $cm^{-2} s^{-1}$ respectively.

3. RESULTS AND DISCUSSION

Five sets of Al/Si samples implanted with energetic Xe^+ were studied by the RBS technique. Of these, a few samples were also studied by channeling, SIMS, NRP and scanning electron microscopy (SEM) techniques. The results of these experiments will be discussed.

3.1. Intermixing

Comparison of RBS spectra of unimplanted samples and samples implanted with a dose of less than 10^{16} ions cm^{-2} definitely indicated that no intermixing occurred. Figure 1(a) shows the RBS spectra of samples implanted with a dose of 2×10^{16} ions cm^{-2} at 150, 200 and 300 keV ion energies. From the parts of the spectra which represent Al/Si we cannot observe any evidence of intermixing. There is, however, some channeling for the silicon substrate of the unimplanted sample.

The profile of xenon implanted with 200 keV energy (Fig. 1(b)) demonstrates that xenon atoms reside in a relatively unmixed double-layer element because (i) the xenon profile is not symmetric (compare Figs. 1(b) and 2(b)) and (ii) the Al–Si interface is clearly demonstrated by a step at a depth of 900 Å. It must be emphasized that the transformation of xenon profile data from energy to depth coordination has been performed using surface energy approximations and the depth–energy loss relationship[16]. For Al–Si systems the depth can be accurately calculated and a knowledge of the aluminum-to-silicon ratio is not a prerequisite. For depths up to 2000 Å, the difference in calculated depth for pure aluminum or silicon for a fixed energy loss of the backscattered $^4He^+$ beam is smaller than the depth resolution of the standard detection system (approximately 250 Å).

In contrast, when one of the samples which was implanted with a dose of 2×10^{16} ions cm^{-2} was re-implanted to a total dose of 6×10^{16} ions cm^{-2} (Fig. 1(c)), the aluminum peak disappeared. The disappearance of the aluminum peak may have two causes: sputtering of aluminum or intermixing of aluminum and silicon. Because the Al–Si edge did not shift completely to where the silicon edge was expected, we can conclude that intermixing has occurred. The small reduction in scattering in the 750–800 keV energy region is due to the relatively high concentration of xenon atoms.

Al/Si samples with a film thickness of 850 Å were also implanted with Xe^+ ions with 250 keV energy to doses of 4.5×10^{16} and 1.1×11^{17} ions cm^{-2}. The RBS spectra in Fig. 2(a) indicate that intermixing occurred. Moreover, the following conclusions can be drawn: (1) the reduction in the scattering in the spectrum of Al/Si xenon implanted at 750–800 keV with a dose of 1.1×10^{17} ions cm^{-2} is due to a high concentration of xenon atoms; (2) the profile (Fig. 2(b)) of implanted xenon with a

dose of 4.5×10^{16} ions cm^{-2} follows a gaussian distribution with a full width at half-maximum (FWHM) of about 900 Å; (3) deviation from the gaussian distribution of the xenon profile (Fig. 2(b)) for a dose of 1.1×10^{17} ions cm^{-2} may have two origins, namely sputtering of target atoms and Xe–Xe collisions (the FWHM for this sample is about 1450 Å); (4) at the half-maximum, the profile of xenon with a dose of 1.1×10^{17} ions cm^{-2} shifted toward the surface by about 400 Å relative to the profile of xenon implanted with a dose of 4.5×10^{16} ions cm^{-2}. Disregarding the range shortening due to the higher implantation dose, we may estimate that a layer 700 Å thick may have sputtered owing to the implantation of 1.1×10^{17} Xe^+ ions cm^{-2}. From these experiments it is not possible to determine the precise value of the sputtering coefficient of aluminum due to energetic Xe^+ ions because the

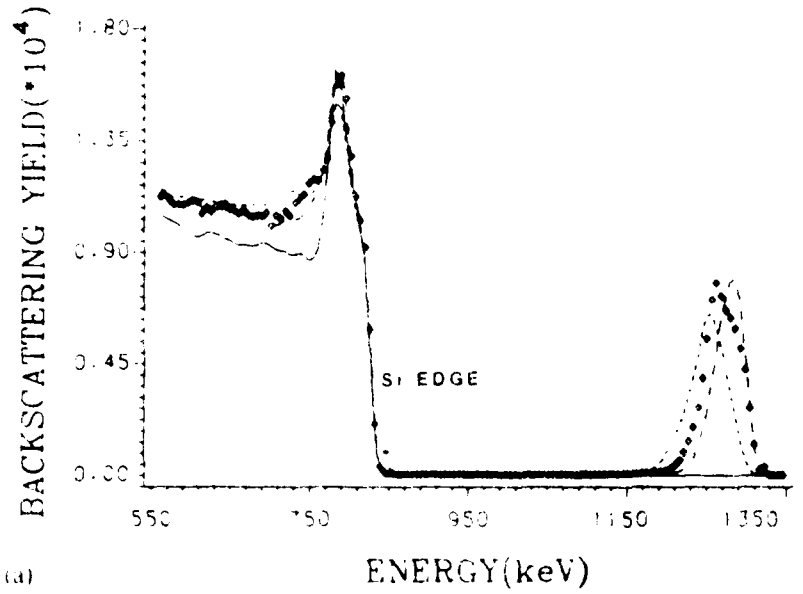

(a)

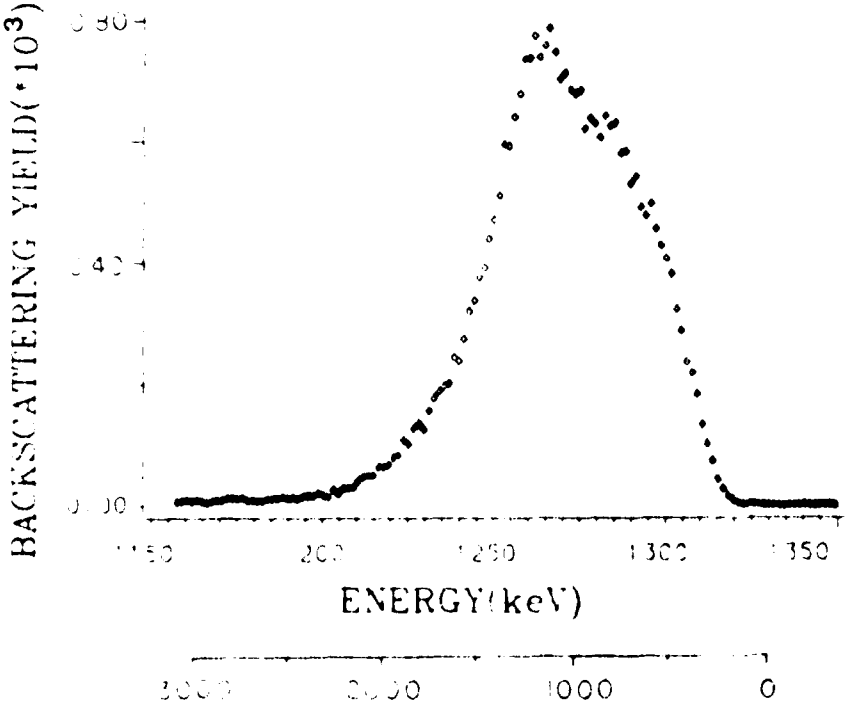

(b)

Fig. 1 (continued)

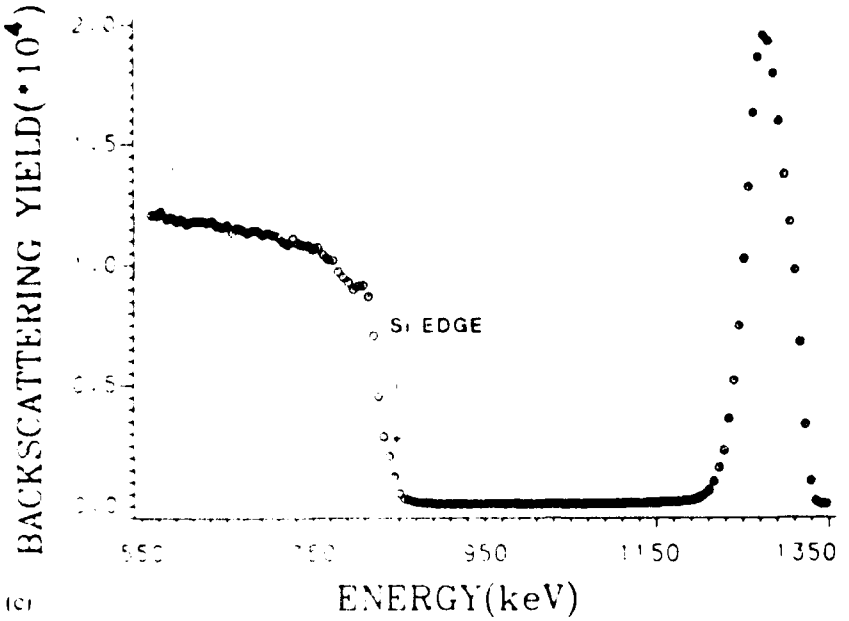

(c)

Fig. 1. 1.5 keV $^4He^+$ RBS spectra of 900 Å aluminum thin films on silicon substrates: (a) samples xenon implanted with a fixed dose (2×10^{16} ions cm^{-2}) and various energies (- - -, 150 keV; ◇, 200 keV; - · -, 300 keV) compared with the unimplanted Al Si system (——); (b) depth profile of xenon implanted with 200 keV energy to a dose of 2×10^{16} ions cm^{-2}; (c) re-implanted sample, where complete intermixing occurred when the dose of implantation was increased (first dose, 2×10^{16} ions cm^{-2} at 150 keV; second dose, 4×10^{16} ions cm^{-2} at 250 keV).

composition of the surface target is subject to change when ion beam mixing is in progress.

3.2. Intermixing and dose rate

Other experiments were performed in order to study the dose rate dependence of Al–Si intermixing. Figure 3 demonstrates RBS spectra of 610 Å of aluminum deposited on silicon substrates implanted with a dose of 4×10^{16} ions cm^{-2} and 200 keV energy and dose rates of 10^{12} and 10^{13} ions cm^{-2} s^{-1}. From these results we can see that, for both samples, aluminum and silicon were equally intermixed. Therefore we can conclude that heat generated during ion implantation is not responsible for the intermixing. There is evidence of self-sputtering of xenon. As can be seen from Fig. 3, the area under the xenon curve for the higher dose rate is diminished by about 15%, although the measured total dose of implantation for both samples was the same.

3.3. Depth profiling by secondary ion mass spectroscopy

Direct observation of aluminum and silicon concentrations in an intermixed layer by RBS is not possible. The sample which was implanted with a low dose rate and described in Section 3.2 and whose RBS spectrum is given in Fig. 3 was studied by SIMS. Figure 4 shows a sputter depth profile taken with SIMS using ^{20}Ne for the sputtering. The starting pressure was about 10^{-8} Torr. The system was then backfilled with ^{20}Ne to about 10^{-5} Torr for sputtering. The (mass 27)-to-(mass 28) intensity ratio is plotted in this figure. If the system were "clean", this should be the ratio of aluminum to silicon. However, there are several problems.

Organics, which are present on the surface, give lines between mass numbers 24

and 30 and hence can contribute to the signal corresponding to mass numbers 27 and 28. Furthermore, with hydrogen present, a part of the peak for mass number 28 could be from AlH. Because the (mass 27)-to-(mass 28) intensity ratio becomes so large (80), we still believe that the data show essentially some residual aluminum as a film and some mixing at the interface. However, the depth scale for aluminum may not be accurate owing to the presence of oxygen and preferential sputtering. It should be emphasized that at a depth beyond the first few hundred ångströms no organic has been observed. Therefore we conclude that the (mass 27)-to-(mass 28)

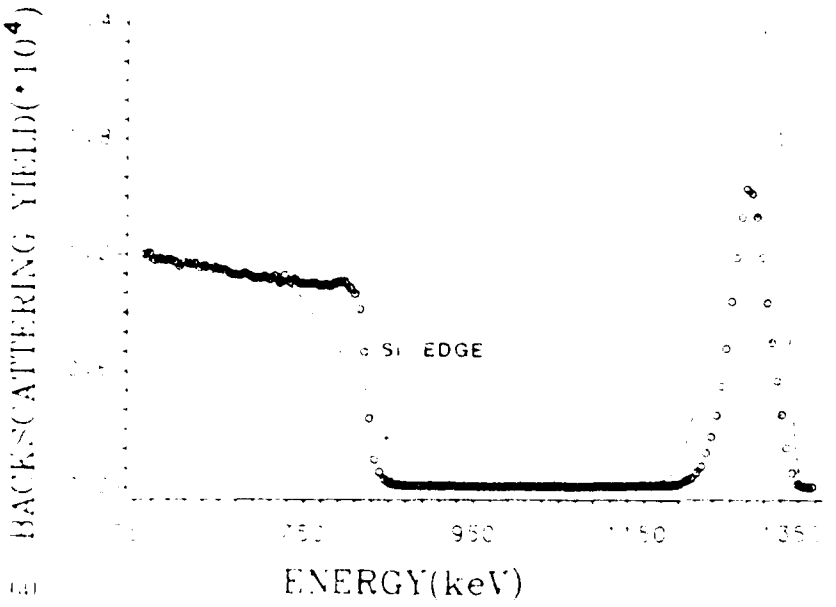

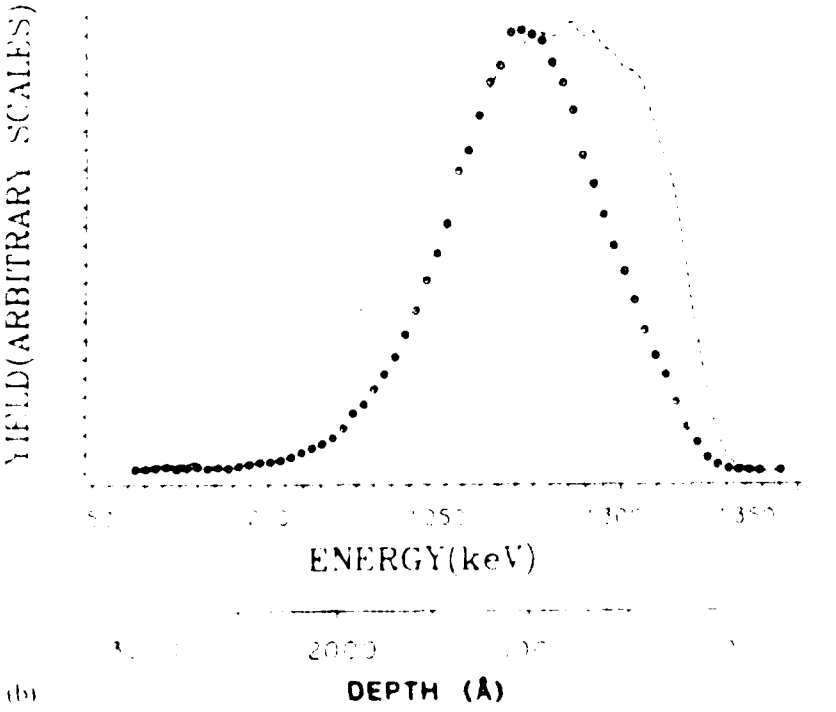

Fig. 2. (a) 1.8 keV $^4He^+$ RBS spectra of an 850 Å aluminum layer on a silicon substrate implanted with xenon with 250 keV energy and doses of 1.1×10^{15} ions cm^{-2} (—) and 4.5×10^{16} ions cm^{-2} (○). (b) Comparison of the depth profile of xenon for these two do[illegible]

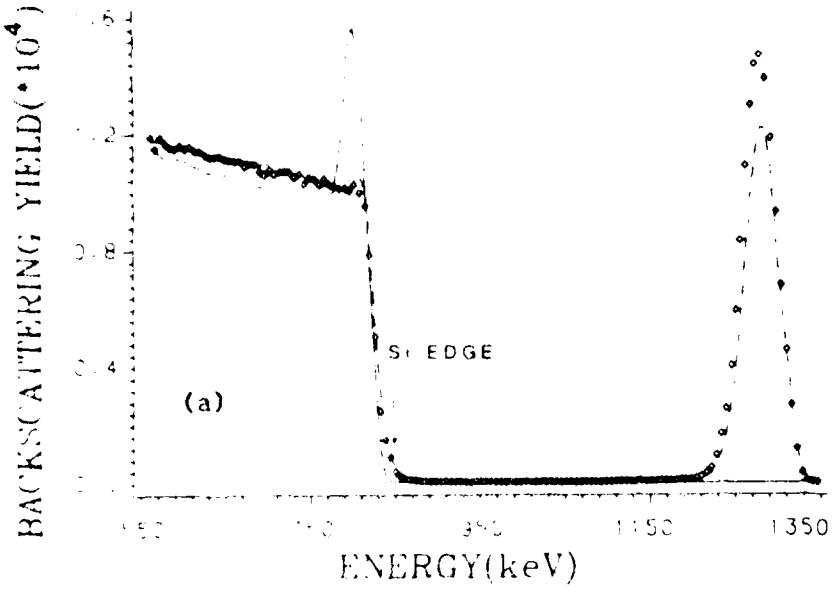

Fig. 3. 1.5 keV $^4He^+$ RBS spectra of 610 Å of aluminum on silicon substrates as deposited (— —) and xenon implanted with 200 keV energy with a fixed dose (4×10^{15} ions cm^{-2}) and two different dose rates: △, 10^{13} ions cm^{-2} s^{-1}; ◇, 10^{14} ions cm^{-2} s^{-1}.

ratio is very close to the aluminum-to-silicon ratio (except for a sensitivity factor). Moreover, there were clear peaks in the SIMS spectra at mass numbers 27 and 28 at a depth of 1000–4000 Å. Therefore, the long tail present in Fig. 4 cannot be due to background; the (mass 27)-to-(mass 28) ratio should eliminate the effect of a very small SIMS background signal.

3.4. Nuclear resonance profiling

The presence of aluminum, as suggested by SIMS, at a depth of 4000 Å should be examined by a technique which would be independent of the sputtering effect. In addition, a knowledge of aluminum depth profiles in surface regions is important in this study. We have therefore examined a few samples by the NRP technique[17].

The broadening of the 992 keV narrow resonance line of the $^{27}Al(p,\gamma)^{28}Si$

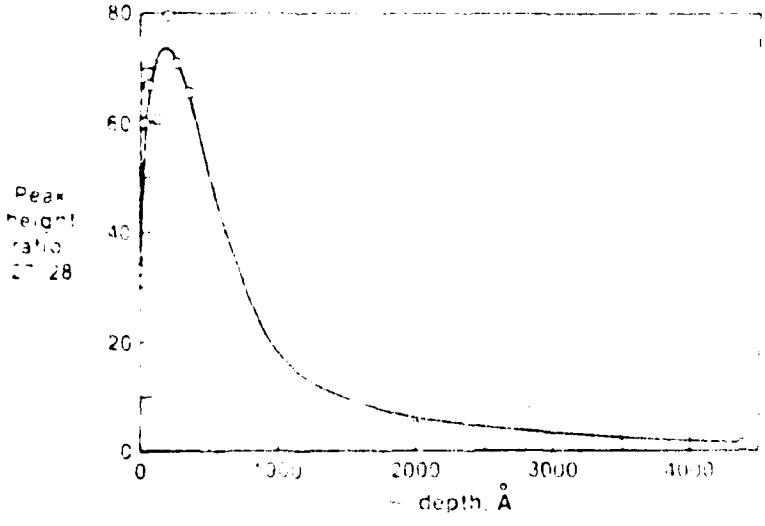

Fig. 4. SIMS sputtering profile of a xenon-implanted 610 Å aluminum layer on a silicon substrate with a dose of 4×10^{15} ions cm^{-2} and 200 keV energy.

reaction[18] has been observed by measuring the intensity of 1.78 MeV γ rays as a function of proton energy. Samples were tilted to 30° with respect to the proton beam and an NaI(Tl) scintillator detector 7.5 cm thick was placed perpendicular to the beam. Figure 5 shows the results for 850 Å of aluminum on silicon both unimplanted and implanted with 250 keV energy and a dose of 10^{17} ions cm^{-2}. Although the upper limit of depth resolution of the system was about 350 Å for the aluminum target, the result is sufficiently accurate to be compared with the SIMS data and the presence of aluminum on the surface region can be positively proven.

The thickness of the aluminum film for the unimplanted sample determined by NRP is about 950 Å which is in good agreement with 850 Å measured by RBS. Figure 5 indicates that about 80% of the aluminum film is sputtered during the xenon implantation. This agrees with the estimate given for sputtered layers at the end of Section 3.1. The presence of aluminum for the intermixed sample up to a depth of 1000 Å is indicated. However, no aluminum can be seen at a depth of 4000 Å. We can therefore conclude that the long tail present in Fig. 4 may be due to preferential silicon sputtering by the neon beam which was used in the SIMS experiment. The channeling experiment discussed below will verify this argument. A very large difference in sputtering rates is probably necessary to explain the persistence of aluminum to 4000 Å in the data. It is probable that a very small amount of oxygen present in the chamber is responsible for a reduction in the aluminum sputtering rate.

3.5. Depth of surface damage

The depth of damage created in the process of ion beam mixing is another important point which has also been explored. From backscattering spectra of a $^4He^+$ beam aligned with one of the silicon crystal axes or planes of the xenon-

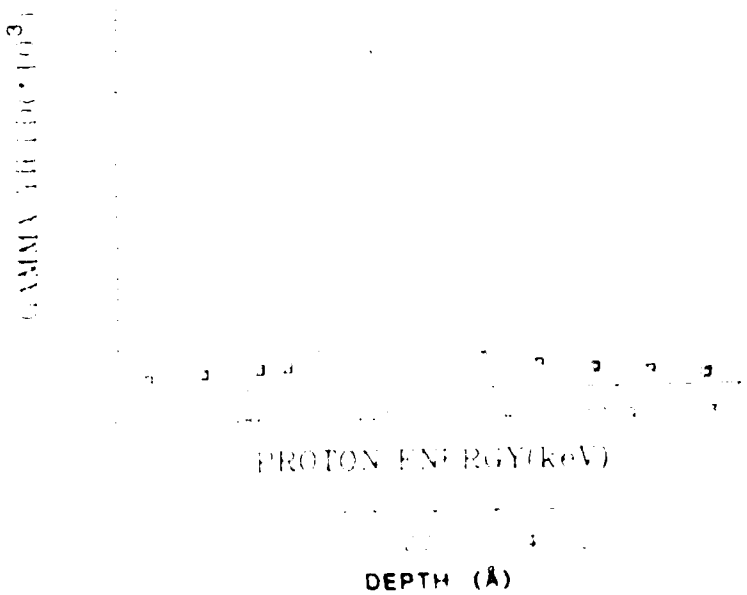

Fig. 5. Depth profile of an 850 Å aluminum layer on Si(111), unimplanted (○) and xenon implanted with a dose of 1.1×10^{17} ions cm^{-2} and 250 keV energy (□), obtained by the NRP technique using the $^{27}Al(p,\gamma)^{28}Si$ reaction.

implanted Al Si system, we can determine the surface damage thickness while the depth profile of xenon can be observed by a simple RBS experiment. We studied unimplanted and xenon-implanted Al/Si(111) samples by means of the channeling technique. The results of these experiments indicate that the damage depth extends almost exactly to the greatest depth at which xenon could be experimentally observed. Beyond this the crystalline structure remains intact.

For example, the damage created by the implantation of xenon with a dose of 1.1×10^{17} and 250 keV is limited to 2000 Å from the surface. Therefore we can conclude that only a few aluminum atoms may have been recoil implanted to a depth beyond 2000 Å simply because the integrity of the crystalline structure beyond 2000 Å was retained. It is well known that implantation with a dose of about 10^{14} ions cm^{-2} destroys the structure of crystalline silicon (see for example ref. 19). Backscattered $^4He^+$ ions from the damage area, from xenon as well as from the as-deposited aluminum films, did not show any angular dependence.

3.6. *Surface study by scanning electron microscopy*

Xenon-implanted Al Si samples annealed at room temperature for a period of 6 months were studied by SEM. Scanning electron micrographs of xenon implanted in 850 Å of aluminum on silicon are given in Figs. 6(b) and 6(d). The surface of the

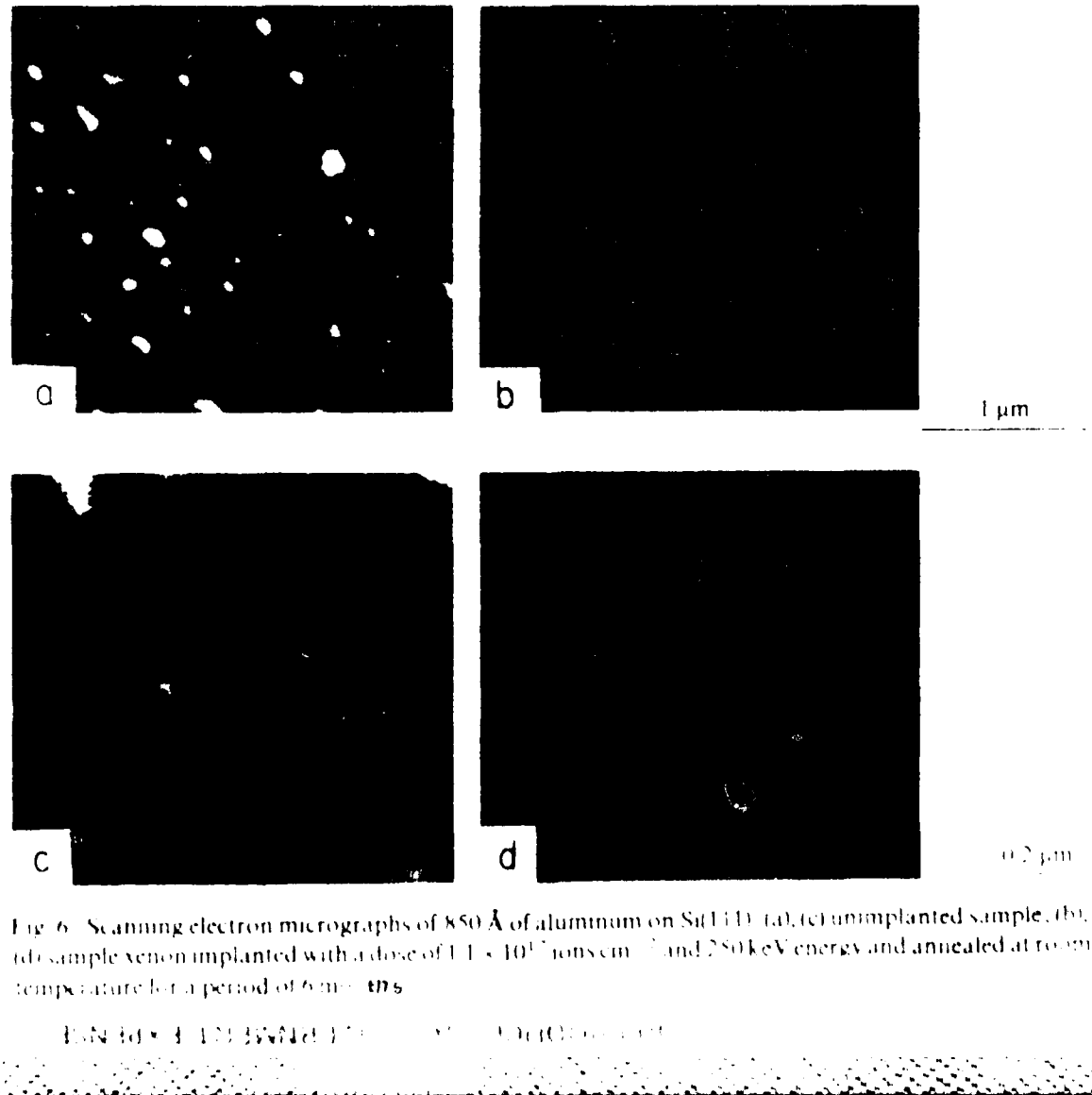

Fig. 6. Scanning electron micrographs of 850 Å of aluminum on Si(111): (a), (c) unimplanted sample; (b), (d) sample xenon implanted with a dose of 1.1×10^{17} ions cm^{-2} and 250 keV energy and annealed at room temperature for a period of 6 months.

sample is uniform in texture and no segregation of aluminum and silicon can be seen. Figures 6(a) and 6(c) show SEM micrographs of 850 Å of unimplanted aluminum on silicon. The origin of the white spots is not well understood. However, we tentatively attribute them to aluminum islands which, on xenon implantation, vanish in the near surface region.

The RBS spectra (see Fig. 2(a)) and NRP results (see Fig. 5) indicate the presence of silicon and aluminum respectively on the sample surface. The SEM micrographs in Figs. 6(b) and 6(d) show that the surface possesses a uniform texture. Therefore we can conclude that the Al–Si alloy layer produced by the ion beam technique retains its integrity after a long period of room temperature annealing. This is in contrast with the Au–Si system which decomposed into an equilibrium mixture of gold and silicon under similar conditions[13].

4. SUMMARIZING REMARKS

We have shown that the implantation of energetic xenon through the interface of aluminum films on silicon substrates can induce intermixing. For our samples whose interfaces were contaminated with oxygen, the dose of implantation had to exceed 2×10^{16} ions cm^{-2}. The requirement of a relatively high dose and the absence of dose rate dependence indicate that recoil implantation is the most likely cause of this intermixing. Surface damage created during ion beam mixing is limited to the maximum penetration depth of xenon ions and possibly a few aluminum atoms were recoil implanted beyond this region. Depth profiling by SIMS shows some mixing at the interface. However, the depth scale is not absolute because of silicon preferential sputtering. Scanning electron micrographs of the annealed sample at room temperature, where the presence of aluminum and silicon on the surface was verified by NRP and RBS, showed no texture in the mixed region, *i.e.* no segregation of aluminum on silicon.

We are in the process of preparing aluminum films on silicon substrates with an oxygen-free interface. We have started to study the stability of an Al–Si alloy at elevated annealing temperatures in order to understand the reason for the stability of these layers and the dependence of the stability on the presence of impurities. As lateral uniformity and stability of the intermixed Al–Si are the most striking features of this work, we believe that, in practice, the ion beam technique can be successfully applied to the production of Al–Si alloy layers near the surface.

ACKNOWLEDGMENTS

We are very grateful to Professor Quentin Kessel for his assistance in various stages of this work.

In addition, we should like to thank John Gianopoulous and Walter Marsh for their technical help.

This work was supported by the U.S. Office of Naval Research.

REFERENCES

1. P. A. Totta and R. P. Sopher, *IBM J. Res. Dev.* **13** (1969) 226.
2. C. H. Lane, *Metall. Trans.* **1** (1970) 713.

3 J. O. McCaldin and H. Sankur, *Appl. Phys. Lett.*, *19* (1971) 524.
4 T. E. Price and L. S. Berthoad, *Solid-State Electron.*, *16* (1973) 1303.
5 K. Chino, *Solid-State Electron.*, *16* (1973) 119.
6 G. J. Van Gurp, *J. Appl. Phys.*, *44* (1973) 2040.
7 J. O. McCaldin and H. Sankur, *Appl. Phys. Lett.*, *20* (1972) 171.
8 H. Sankur, J. O. McCaldin and J. DeVaney, *Appl. Phys. Lett.*, *22* (1973) 64.
9 T. M. Reith and J. D. Shick, *Appl. Phys. Lett.*, *25* (1974) 524.
10 R. L. Boatright and J. O. McCaldin, *J. Appl. Phys.*, *47* (1976) 2260.
11 B. Y. Tsaur, Z. L. Liau and J. W. Mayer, *Appl. Phys. Lett.*, *34* (1979) 168.
12 T. Kanayama, H. Tanoue and T. Tsurushima, *Appl. Phys. Lett.*, *35* (1979) 222.
13 B. Y. Tsaur, J. W. Mayer, M.-A. Nicolet and K. N. Tu, in J. K. Hirvonen and C. M. Preece (eds.), *Surface Modification of Materials by Ion Implantation*, Materials Research Society, University Park, PA, 1979.
14 F. Namavar, *Doctoral Thesis*, University of Leuven, Leuven, 1978.
F. Namavar, M. Rots, J. Gaes and R. Coussement, *Hyperfine Interact.*, *12* (1982) 233.
15 S. R. Reintsema, E. Verbrest, J. Odeurs and H. Pattyn, *J. Phys. E*, *9* (1979) 1511.
16 W.-K. Chu, J. W. Mayer and M.-A. Nicolet, *Backscattering Spectroscopy*, Academic Press, New York, 1978.
17 W. R. Philips and F. H. Read, *Proc. Phys. Soc. London*, *81* (1963) 1.
18 R. O. Bondelid and C. A. Kennedy, *Phys. Rev.*, *115* (1959) 1601.
S. J. Skorka and T. W. Retz-Schmidt, *Nucl. Phys.*, *46* (1963) 225.
19 E. T. Yeng, B. J. Masters and R. Kastl, in S. Namba (ed.), *Ion Implantation in Semiconductors*, Plenum, New York, 1975.

END

FILMED

9-85

DTIC